



Minerva Access is the Institutional Repository of The University of Melbourne

Author/s:

Pidot, SJ; Klatt, S; Ates, LS; Frigui, W; Sayes, F; Majlessi, L; Izumi, H; Monk, IR; Porter, JL; Bennett-Wood, V; Seemann, T; Otter, A; Taiaroa, G; Cook, GM; West, N; Tobias, NJ; Fuerst, JA; Stutz, MD; Pellegrini, M; McConville, M; Brosch, R; Stinear, TP

Title:

Marine sponge microbe provides insights into evolution and virulence of the tubercle bacillus

Date:

2024-08-01

Citation:

Pidot, S. J., Klatt, S., Ates, L. S., Frigui, W., Sayes, F., Majlessi, L., Izumi, H., Monk, I. R., Porter, J. L., Bennett-Wood, V., Seemann, T., Otter, A., Taiaroa, G., Cook, G. M., West, N., Tobias, N. J., Fuerst, J. A., Stutz, M. D., Pellegrini, M., ... Stinear, T. P. (2024). Marine sponge microbe provides insights into evolution and virulence of the tubercle bacillus. *Plos Pathogens*, 20 (8), <https://doi.org/10.1371/journal.ppat.1012440>.

Persistent Link:

<https://hdl.handle.net/11343/358482>

License:

CC BY

RESEARCH ARTICLE

Marine sponge microbe provides insights into evolution and virulence of the tubercle bacillus

Sacha J. Pidot^{1*}, Stephan Klatt^{2a}, Louis S. Ates³, Wafa Frigui³, Fadel Sayes³, Laleh Majlessi³, Hiroshi Izumi⁴, Ian R. Monk¹, Jessica L. Porter¹, Vicki Bennett-Wood¹, Torsten Seemann¹, Ashley Otter⁵, George Tairaoa⁶, Gregory M. Cook⁶, Nicholas West⁴, Nicholas J. Tobias¹, John A. Fuerst⁴, Michael D. Stutz⁷, Marc Pellegrini⁷, Malcolm McConville², Roland Brosch³, Timothy P. Stinear^{1*}

1 Department of Microbiology and Immunology, Peter Doherty Institute for Infection and Immunity, University of Melbourne, Melbourne, Australia, **2** Department of Molecular Biology and Biochemistry, Bio21 Institute, University of Melbourne, Parkville, Australia, **3** Institut Pasteur, Université Paris Cité, Unit for Integrated Mycobacterial Pathogenomics, Paris, France, **4** School of Chemistry and Molecular Biosciences, University of Queensland, Brisbane, Australia, **5** UK Health Security Agency, Porton Down, Salisbury, United Kingdom, **6** Department of Microbiology and Immunology, University of Otago, Dunedin, New Zealand, **7** Walter and Eliza Hall Institute of Medical Research, Parkville, Australia

^a Current address: Institute for Vascular Signalling, Centre of Molecular Medicine, Goethe University Frankfurt, Germany

* sacha.pidot@unimelb.edu.au (SJP); tstinear@unimelb.edu.au (TPS)



OPEN ACCESS

Citation: Pidot SJ, Klatt S, Ates LS, Frigui W, Sayes F, Majlessi L, et al. (2024) Marine sponge microbe provides insights into evolution and virulence of the tubercle bacillus. *PLoS Pathog* 20(8): e1012440. <https://doi.org/10.1371/journal.ppat.1012440>

Editor: Thomas Hawn, University of Washington, UNITED STATES OF AMERICA

Received: April 30, 2024

Accepted: July 22, 2024

Published: August 29, 2024

Copyright: © 2024 Pidot et al. This is an open access article distributed under the terms of the [Creative Commons Attribution License](https://creativecommons.org/licenses/by/4.0/), which permits unrestricted use, distribution, and reproduction in any medium, provided the original author and source are credited.

Data Availability Statement: The *M. spongiae* genome sequence is available at Genbank with the accession CP046600. All other relevant data are within the manuscript and its [Supporting Information](#) files.

Funding: This project was supported by a National Health and Medical Research Council (NHMRC) Ideas grant (GNT2021638) to S.J.P., a NHMRC L2 Fellowship to T.P.S., and NHMRC Project Grant (GNT1105522) to T.P.S. and S.J.P., an Agence Nationale pour la Recherche grant (ANR-10-LABX-

Abstract

Reconstructing the evolutionary origins of *Mycobacterium tuberculosis*, the causative agent of human tuberculosis, has helped identify bacterial factors that have led to the tubercle bacillus becoming such a formidable human pathogen. Here we report the discovery and detailed characterization of an exceedingly slow growing mycobacterium that is closely related to *M. tuberculosis* for which we have proposed the species name *Mycobacterium spongiae* sp. nov., (strain ID: FSD4b-SM). The bacterium was isolated from a marine sponge, taken from the waters of the Great Barrier Reef in Queensland, Australia. Comparative genomics revealed that, after the opportunistic human pathogen *Mycobacterium decipiens*, *M. spongiae* is the most closely related species to the *M. tuberculosis* complex reported to date, with 80% shared average nucleotide identity and extensive conservation of key *M. tuberculosis* virulence factors, including intact ESX secretion systems and associated effectors. Proteomic and lipidomic analyses showed that these conserved systems are functional in FSD4b-SM, but that it also produces cell wall lipids not previously reported in mycobacteria. We investigated the virulence potential of FSD4b-SM in mice and found that, while the bacteria persist in lungs for 56 days after intranasal infection, no overt pathology was detected. The similarities with *M. tuberculosis*, together with its lack of virulence, motivated us to investigate the potential of FSD4b-SM as a vaccine strain and as a genetic donor of the ESX-1 genetic locus to improve BCG immunogenicity. However, neither of these approaches resulted in superior protection against *M. tuberculosis* challenge compared to BCG vaccination alone. The discovery of *M. spongiae* adds to our understanding of the emergence of the *M. tuberculosis* complex and it will be another useful resource to refine

62-IBEID) to RB and an Australian Research Council (ARC) Linkage project (LP0882233) to J.A. F. H.I. was supported by a University of Queensland Research Scholarship (UQRS) and University of Queensland International Research Tuition Award (UQIRTA). The funders had no role in study design, data collection and analysis, decision to publish, or preparation of the manuscript.

Competing interests: The authors have declared that no competing interests exist.

our understanding of the factors that shaped the evolution and pathogenesis of *M. tuberculosis*.

Author summary

Tuberculosis, caused by *Mycobacterium tuberculosis*, is still one of the world's deadliest infectious diseases. However, the origins and rise of *M. tuberculosis* as a successful pathogen are not well understood. Here, we report the isolation and characterisation of a marine sponge-derived mycobacterium (*M. spongiae*) from the Great Barrier Reef that has striking genotypic similarity to *M. tuberculosis*, with 80% average nucleotide identity. We further show by proteomic and lipidomic analyses that *M. spongiae* shares virulence factors and unique cell wall lipids with the tubercle bacillus. In spite of these conserved genotypic and phenotypic features, *M. spongiae* was not virulent in a mouse model of infection, leading us to investigate its potential as a vaccine strain or genetic donor for enhancing the current BCG vaccine for tuberculosis. Our findings contribute to understanding the evolutionary origins of *M. tuberculosis* and provide further insights into its pathogenesis.

Introduction

M. tuberculosis, the causative agent of human tuberculosis (TB), is the leading bacterial cause of mortality and morbidity worldwide and is responsible for approximately 1.5 million deaths per year [1]. Tuberculosis has affected humans since at least the neolithic expansion of humans across the continents. Despite the wealth of molecular evidence explaining the evolution of mycobacteria that cause tuberculosis in humans and other mammals (the *Mycobacterium canettii* clade and *M. tuberculosis* complex, MTBC), the origins of this complex and their differentiation from other mycobacteria are only beginning to be understood.

Several environmental mycobacteria have also been noted as close ancestors of the MTBC, including *Mycobacterium marinum*, a fish and human pathogen [2], and *Mycobacterium kansasii* [3], although neither of these mycobacteria have been seen to transmit between humans and they have significantly larger genomes than *M. tuberculosis*. Recent genomic analyses have identified some other opportunistic human pathogens, such as *Mycobacterium riyhadense*, *Mycobacterium lacus*, *Mycobacterium shinjukense* and *Mycobacterium decipiens*, that share many features of host-adaptation with *M. tuberculosis* [4]. However, these closely related, slow growing non-tuberculous mycobacteria (NTM) bacteria differ in many aspects from tuberculosis-causing mycobacteria. These studies suggest that there are likely other taxa to discover that can aid our understanding of *M. tuberculosis* evolution from a generalist mycobacterium into a highly virulent, specialist human pathogen.

Marine sponges are known to house a large and diverse repertoire of bacteria, as attested by recent efforts to catalogue the microbiome of these animals from around the world [5–7]. These studies have shown that Actinobacteria are one of the largest phyla within these microbial communities. As part of efforts to identify and catalogue Actinobacterial symbionts from marine sponges on the Great Barrier Reef in Australia, and to identify possible target species of anti-mycobacterial rifamycins produced by *Salinospora* sponge symbionts, a mycobacterial isolate named FSD4b-SM was isolated from a *Fascaplysinopsis reticulata* sponge at a depth of

25m [8]. Initial investigations of this strain showed that it was closely related to the MTBC by conserved gene amplicon sequencing [8].

Here, we sought to better understand the genetic and functional relationships between FSD4b-SM and the MTBC through genomic, proteomic and lipidomic analyses. Our research establishes FSD4b-SM as the most closely related marine organism to the MTBC, assesses its virulence potential, and its prospects for use in TB vaccine development.

Results and discussion

General characterisation of *Mycobacterium spongiae* FSD4b-SM

We first performed general phenotypic analyses of *M. spongiae* FSD4b-SM that showed it was capable of growth on solid media typically used for culturing heterotrophic marine bacteria, although colony formation was scant (Fig 1A). FSD4b-SM did not grow on media typically used for mycobacterial growth, such as Lowenstein-Jensen or egg-yolk-based agar media. An analysis of growth performed in simplified marine broth, showed that FSD4b-SM grew

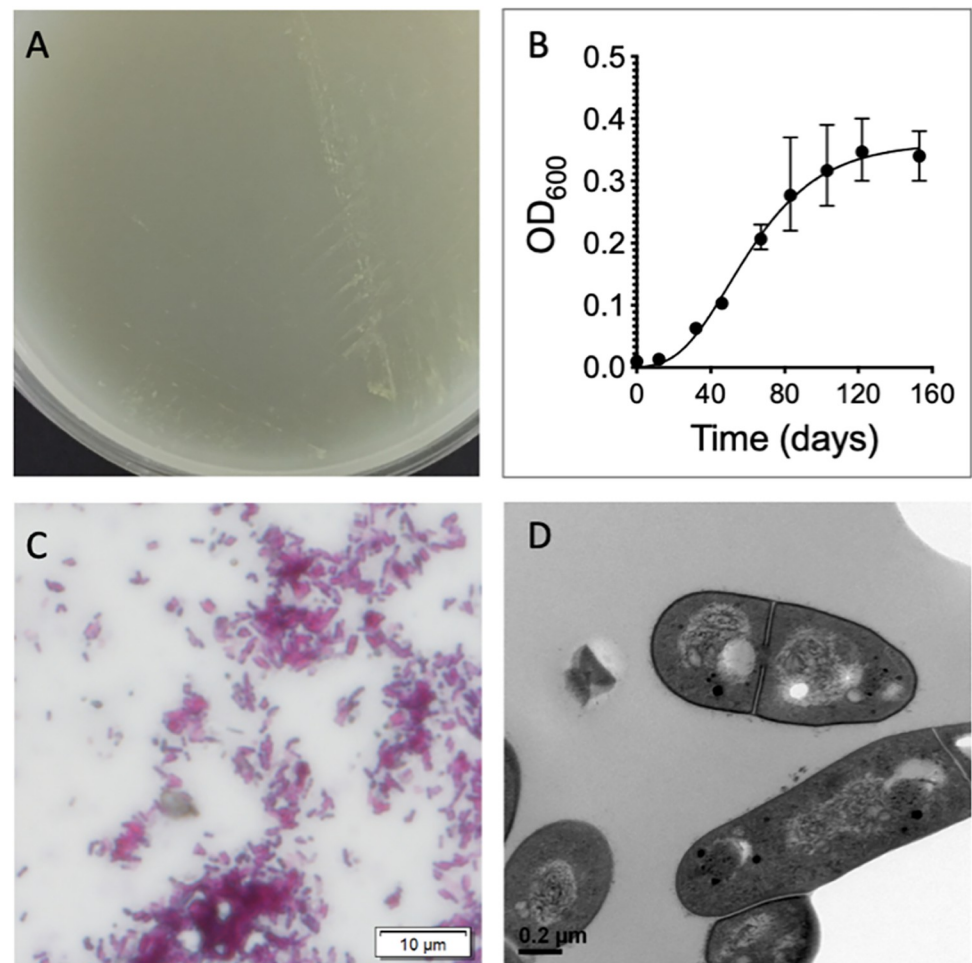


Fig 1. General phenotypic characteristics of *Mycobacterium* strain FSD4b-SM. A) Representative example of scant *M. spongiae* growth on simplified marine agar. B) Growth curve of *M. spongiae* in simplified marine broth. Each point is an average of measurements taken from three biological replicates (S2 Table). C) Ziehl-Neelsen stained *M. spongiae* cells. D) Electron micrograph of *M. spongiae* cells (x 33,000 magnification).

<https://doi.org/10.1371/journal.ppat.1012440.g001>

optimally at 28°C with an estimated doubling time of 64 days and reached stationary phase after approximately three months (Fig 1B). FSD4b-SM was unable to grow at 37°C. The bacteria stained acid-fast, forming short, compact rods (Fig 1C). Transmission electron microscopy confirmed rod-shaped cells, approx. 2 µm in length and 0.4 µm in diameter (Fig 1D).

Comparative genomics of *Mycobacterium spongiae* FSD4b-SM with other mycobacteria

Comparative genomics between related mycobacteria has provided significant insights into the factors that make *M. tuberculosis* pathogenic. Previous work using partial, concatenated 16S rRNA, *hsp65* and *rpoB* gene sequences from FSD4b-SM showed that it was closely related to the MTBC [8]. To gain greater insight into the relationship between FSD4b-SM, the MTBC and other mycobacterial species, we first completed a high-quality, closed FSD4b-SM genome using a combination of Illumina and PacBio sequencing. FSD4b-SM has a single circular 5,581,157 bp chromosome, harbouring 4458 coding sequences (CDS) (134 predicted pseudo-genes) and a single rRNA locus. The average GC percentage was 65.56%. Initial comparisons of genome size showed that the FSD4b-SM genome is 1.1 Mb larger than the *M. tuberculosis* H37Rv genome (4.4Mb) [9,10], but smaller than other close *M. tuberculosis* relatives, such as *Mycobacterium kansasii* (6.4 Mb) [11] and *Mycobacterium marinum* (6.6 Mb) [2].

To explore the relationship between FSD4b-SM and other mycobacteria more thoroughly, we calculated pairwise average nucleotide identity (ANI) with *M. tuberculosis* and eight other mycobacterial species known to be closely related to the MTBC (Fig 2A). This analysis compares nucleotide identity between two genomes, with FSD4b-SM clustering most closely with *M. decipiens* and the MTBC (represented by *M. tuberculosis* and *M. canettii*) (approx. 80% ANI) (Fig 2A). However, the overall ANI differences between all 10 mycobacterial genomes were minimal and cluster resolution was subsequently low (Fig 2A). To improve resolution and gain greater insight into evolutionary relationships between FSD4b-SM, the MTBC and other mycobacteria we inferred a phylogeny among the same 10 mycobacteria and included an additional 20 comparator mycobacterial genomes (Fig 2B) [4]. We built a maximum-likelihood phylogeny from amino acid sequence alignments of 107 essential, single-copy core CDS that are found in the majority of bacteria [12]. This analysis showed that among all 30 mycobacterial genomes FSD4b-SM clusters with *Mycobacterium decipiens* and the MTBC, within a group of mycobacteria previously defined as the *M. tuberculosis*-associated phylotype (MTBAP) and consistent with the ANI results (Fig 2B) [4]. The relatively long branch length of FSD4b-SM within the MTBAP cluster supports the classification of this mycobacterium as a distinct species (Fig 2B). To delve further into the relationship between *M. tuberculosis* and FSD4b-SM, we more closely assessed core genome differences between these two mycobacteria and the genomes from three other key mycobacterial species (*M. kansasii*, *M. marinum*, and *M. decipiens*) (Fig 2C). The five species shared a core genome of 1815 CDS, with FSD4b-SM sharing more than 50% of its CDS content with *M. marinum*, despite being more distantly related at the nucleotide level (Fig 2C). However, *M. spongiae* and *M. tuberculosis* also share approximately 55% of their coding capacity (*c.f.* *M. tuberculosis* and *M. marinum*, which also share 55% coding capacity); it is notable that a mammalian host-restricted pathogen like *M. tuberculosis* shares much of its protein coding capacity with marine mycobacteria. Overall chromosome architecture is well conserved between FSD4b-SM and the closely related species, but there are also several regions spanning approximately 500kb in total of the FSD4b-SM genome that are distinct to the sponge mycobacterium (Fig 2D and 2E). Upon further investigation it was noted that several of these distinct regions harboured large gene clusters encoding putative polyketide synthase (PKS) or non-ribosomal synthetase (NRPS) enzymes. These

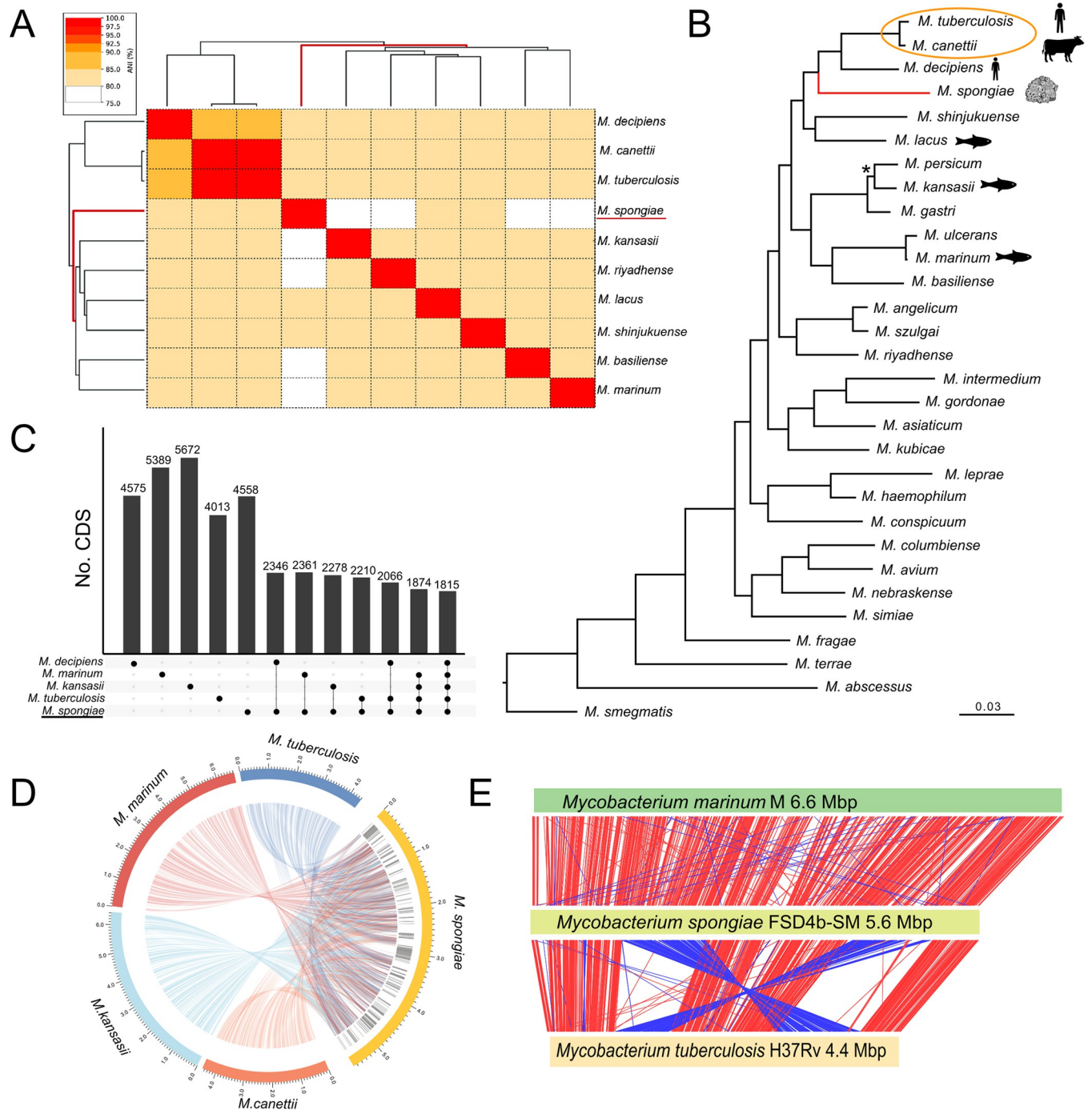


Fig 2. Comparative genomics summary of *Mycobacterium spongiae* FSD4b-SM. A) Pairwise average nucleotide identity (%ANI) between related *Mycobacterium* species. B) Maximum-likelihood phylogenetic tree (*iqtree*) with 1000 bootstrap iterations, inferred among 30 mycobacteria and based on amino acid sequence alignments from 107 conserved bacterial genes (*bcgTree*). *M. smegmatis* was used as an outgroup to root the phylogeny. Asterisk indicates node with >60% bootstrap support. All other tree nodes had greater than 90% bootstrap support. MTBC encircled. Red branch length denotes *M. spongiae* FSD4b-SM placement. C) Upset plot showing shared coding sequences (CDS) at the 80% amino acid identity level between five related mycobacteria (*Roary*). D) Circos plot showing DNA sequence homology (*Blastn*) among *M. spongiae* and closely related species. Regions on the outermost ring represent the length of each individual genome, grey shading on the next innermost ring shows regions that are unique to *M. spongiae* among these comparator genomes. Links from the *M. spongiae* genome to other genomes show relative positions of regions encoding orthologues with >80% amino acid similarity. Link colours correspond to the colour of each genome on the outermost ring. E) Artemis Comparison Tool (ACT) plot showing comparative chromosome architecture between *M. spongiae*, *M. marinum* and *M. tuberculosis*. Links between the sequences denote regions with >75% nucleotide identity, with red links indicating the same DNA orientation, while blue links indicate inverse orientation with respect to each genome.

<https://doi.org/10.1371/journal.ppat.1012440.g002>

enzymes are involved in the production of specialised metabolites in bacteria and fungi, including many well-known bioactive molecules, such as antibiotics and anticancer compounds [13]. To assess these PKS- and NRPS-encoding regions further, we utilised the bioinformatic tool antiSMASH to predict regions of the genome likely to be involved in specialised metabolism [14]. This analysis identified 19 regions of DNA predicted to encode proteins involved in specialised metabolism in the FSD4b-SM genome. As PKSs are heavily involved in the biosynthesis of core mycobacterial lipids, such as the mycoketides, phthiocerol dimycoserates and mycolic acids (discussed in detail below), the majority of these 19 regions are well conserved across a range of mycobacteria. The FSD4b-SM genome also encodes an orthologous NRPS locus for the production of isonitrile lipopeptides (INLPs) (F6B93_01120–01155), which are used by *M. tuberculosis* and other pathogenic mycobacteria for metal transport [15]. However, five of these 19 specialised metabolite loci appear to be specific to FSD4b-SM, corresponding to a total of 315 kb of DNA. These include a hybrid PKS-NRPS locus that has greater homology to PKS-NRPS systems from algae than those from other mycobacteria (F6B93_00330 –F6B93_00460); a putative alkylresorcinol locus (F6B93_10605 –F6B93_10760), that are known to produce molecules with antioxidant, cytotoxic or also have signalling properties [16]; and three further PKS-encoding regions (F6B93_18505 –F6B93_18675, F6B93_19200 –F6B93_19380, F6B93_21085 –F6B93_21320) with unknown predicted products. At present it is not possible to predict the final molecular structures of a given PKS from genome sequence information alone, meaning that these regions await the identification of their ultimate chemical entities.

Overview of shared *M. spongiae* and *M. tuberculosis* genetic features

Given the high level of genetic similarity and shared protein orthologues between *M. spongiae* and the MTBC, we sought to identify the presence of known *M. tuberculosis* pathogenesis factors in the FSD4b-SM genome. The *M. tuberculosis* antigens MPT83, TB8.4, antigen 85 complex, ESAT-6 and CFP-10, were all identified in the *M. spongiae* genome with >78% amino acid identity (S5 Table). All four mammalian cell entry (Mce) families present in *M. tuberculosis* are conserved in gene content and synteny in FSD4b-SM, as well as a distinct *mce* locus not found in either *M. tuberculosis* or *M. marinum* (F6B93_18965 to F6B93_18990) [17] (S5 Table). Other conserved pathogenic factors include the ESX secretion systems and a range of key mycobacterial lipid species (both discussed in detail below). Conserved regulatory systems include the PhoPR virulence regulatory system [18,19] and several TetR-family regulators involved in *M. tuberculosis* antibiotic resistance such as EthR (and the associated monooxygenase EthA linked to ethionamide resistance), InhR (isoniazid) and EtbR (isoniazid and ethambutol) [20].

In *M. tuberculosis* the DosS-DosT/DosR (DevST/R) regulatory system controls approximately 50 CDS involved in responses to carbon monoxide (CO) and nitric oxide (NO) exposure [21]. In FSD4b-SM a DosR ortholog exists (F6B93_06220), while F6B93_12710 is a putative sensor kinase most closely related to the *M. tuberculosis* hypoxia sensor DosT (76% amino acid identity). A DosS orthologue appears absent in FSD4b-SM suggesting an inability to sense redox signals in the same way as *M. tuberculosis* [22]. Other *M. tuberculosis* pathogenic determinants that are not well conserved in FSD4b-SM include a sphingomyelinase (encoded by Rv0888) that is used to degrade the major eukaryotic lipid sphingomyelin, and the *M. tuberculosis* outer-membrane channel protein and necrotizing exotoxin CpnT (Rv3903c), whose orthologue in FSD4b-SM (F6B93_13125) shares only 56% aa identity with only the NAD⁺-glycohydrolase domain of Rv3903c [23–25].

The MTBC has more than 80 toxin-antitoxin (TA) systems, important for bacterial persistence within the host. FSD4b-SM has a smaller and distinct toxin-antitoxin repertoire

compared to the MTBC, with only 11 type II TA systems (F6B93_: 00510/00515, 00780/00785, 03975, 12335, 12350, 12355/12360, 13370/13375, 14995/15000, 15135, 18675/18680, 19810/19815). There are also no plasmids, phage or other insertion sequence elements in the FSD4b-SM genome in contrast to *M. tuberculosis* where mobile elements make up 3.4% of its genome [26]. The absence of mobile DNA is also in contrast to the plasmids and prophage that appear in strains of *M. marinum* and *M. kansasii* [2,3]. This suggests that foreign DNA uptake has been restricted in FSD4b-SM. The FSD4b-SM genome contains a number of antibiotic resistance determinants (such as RbpA and aminoglycoside 2'-N-acetyltransferase) that are also present in *M. tuberculosis* [27,28], inferring that these determinants are ancestral to this lineage of mycobacteria.

DNA methylation in FSD4b

The absence of prophage, insertion sequence elements and plasmids suggest strong barriers in FSD4b-SM to extracellular DNA acquisition. DNA restriction modification is one possible barrier, so we took advantage of the PacBio sequence data to explore adenine DNA methylation patterns in this mycobacterium. We observed three different methylated motifs, two previously reported in *M. tuberculosis*, including the highly methylated CTCAG/CTGGAG motif (2582/2592 sites), and GTAYN4ATC (538/565 sites) (S6 Table) [29]. A third FSD4b-SM motif AGCN5CTTC/GAAGN5GCT (624/625 sites) is different to the third *M. tuberculosis* motif (S6 Table). Interestingly, all three motifs had near complete methylation, suggesting efficient methylases working with their cognate (and presumably highly active) restriction modification systems.

FSD4b-SM energetics

There is extensive conservation in FSD4b-SM with *M. tuberculosis* CDS encoding key proteins required for respiration and ATP synthesis, with CDS encoding all key proteins associated with the mycobacterial electron transport chain and the F₁F_o ATP synthase present and intact (S1 Fig). However, like other mycobacteria outside the MTBC, a specific fumarate reductase complex (FrdABCD) is absent in *M. spongiae*. Also, the single nitrate reductase locus *nar* (F6B93_02320—F6B93_02360) is distinct to that found in *M. tuberculosis*. The *M. tuberculosis hyc* hydrogenase locus encoding a purported formate hydrogenylase enzyme complex is also absent in FSD4b-SM [30]. *M. spongiae* instead carries a locus encoding a group 1h hydrogenase complex (F6B93_RS07495—F6B93_RS07595), orthologous to the *hhy* locus in *M. smegmatis* [31]. This complex is presumably used by FSD4b-SM to oxidize molecular hydrogen that is abundant in seawater [32,33].

ESX systems

ESX (or type VII) secretion systems allow mycobacteria to export virulence determinants and other substrates across their specialized cell envelope. Most pathogenic mycobacteria contain up to five of these ESX systems, which are believed to have evolved by horizontal transfer and gene duplication events [34]. The best studied of these systems is ESX-1, which is used by *M. tuberculosis* to permeabilize the phagolysosome and is also responsible for the processing and secretion of two key virulence determinants, CFP-10 (*esxB*) and ESAT-6 (*esxA*). All components of ESX-1 are highly conserved in FSD4b-SM, including CFP-10 and ESAT-6 orthologues (S2 Fig and S7 Table). Additionally, the FSD4b-SM ESX-1 locus contains a nine gene insertion that harbours novel PE and PPE encoding genes (S2 Fig). The four remaining ESX loci are all well conserved in the FSD4b-SM genome and include the components necessary for iron

siderophore uptake (ESX-3, [35]) and for mycobacterial outer membrane permeability and nutrient uptake (ESX-5, [36]).

To investigate whether these ESX systems were functional in FSD4b-SM, we first performed secretion analysis followed by SDS-PAGE as well as Western blot analysis with an array of antibodies against *M. tuberculosis* proteins that are secreted by ESX-secretion systems or commonly used loading controls. While we were unable to detect any specific protein using SigA, GroEL, EsxN, EspA, EsxA (ESAT-6), EsxB (CFP-10), staining with an antibody against PE_PGRS proteins revealed that this group of proteins is highly expressed by FSD4b-SM (S3 Fig). High levels of the proteins were also detected in the culture filtrate. Compared to *M. tuberculosis* fractions the expression of PE_PGRS proteins appear at higher molecular weights, which is like *M. marinum*, another marine-associated mycobacterium [37,38].

To investigate expressed proteins in more detail, we performed proteomic analysis of cell free culture supernatants and whole cell lysates. These analyses confidently identified a total of 1354 expressed proteins, including several proteins of the ESX-1, ESX-2 and ESX-5 secretion systems (S7 Table). ESX-1 substrates and components detected included the major secreted *M. tuberculosis* antigen CFP-10 (F6B93_22245), the chaperone EspB (F6B93_22290), the PE protein chaperone EspG1 (F6B93_22210) and the ESX-1 secretion regulator EspI (F6B93_22255) [39–42]. The ESX-5 secretion system has been shown to be essential to slow growing mycobacteria [36,43] and several substrates of this system were detected, including a full-length version of the substrate EsxM (F6B93_11055), which has been suggested to promote tissue dissemination in ancestral *M. tuberculosis* lineages [44]. In addition, proteins constituting the building blocks of the ESX-5 secretion apparatus were also detected, including EccB5 (F6B93_11005), EccC5 (F6B93_11010), EccD5 (F6B93_11065) and EccE5 (F6B93_11075) (S7 Table) [45]. These results suggest a degree of conservation among type VII secretion systems and functionality between *M. tuberculosis* and the sponge mycobacterium.

PE/PPE proteins

In addition to substrates encoded within each ESX locus, each ESX system also secretes its own array of PE/PPE substrates, so named for the highly conserved Proline-Glutamate and Proline-Proline-Glutamate motifs present in their N-termini, respectively [46]. While PE/PPE proteins are found across both saprophytic and pathogenic mycobacteria, the latter generally harbour more of these proteins and in *M. tuberculosis* they are implicated in diverse phenotypes, including nutrient acquisition, and a range of pro- and anti-immunity responses [35,46–48]. Several *M. tuberculosis* PE/PPE proteins are essential for bacterial growth under a range of *in vitro* and *in vivo* conditions [49,50]. Examination of the FSD4b-SM genome identified 179 PE and 82 PPE genes (S8 Table) corresponding to over 10% of its coding capacity, compared to 99 PE and 69 PPE genes in *M. tuberculosis* (7% of the genome) [9,46]. This repertoire includes multiple members of the PE_PGRS and PE_MPTR subfamilies that are restricted to members of the MTBC [46,51] and is consistent with the expansion of PE/PPE family proteins in slow growing mycobacteria [52].

FSD4b-SM contains a number of orthologues to PE/PPE proteins reported to have important roles in *M. tuberculosis* growth including PPE4 (F6B93_02120) and its secretion partner PE5 (F6B93_02115), that participate in mycobactin-mediated iron acquisition [35,53,54], PPE62 (F6B93_06010) involved in heme and hemoglobin utilisation [55], and PE19 (F6B93_11045) associated with stress resistance (S8 Table) [56]. Likewise, multiple *M. tuberculosis* PPEs that are involved in virulence have orthologues in *M. spongiae* including PPE25 (F6B93_11025), PPE26 (F6B93_11035), PPE27 (F6B93_04645), PPE68 (F6B93_22240) and PE35 (F6B93_11875) [57–59]. FSD4b-SM also possesses a number of PE/PPE proteins that

have been positively linked to the secretion of type VII substrates, including PPE38 (F6B93_14895), which is essential for the secretion of PPE_MPTR and PE_PGRS proteins in the *M. tuberculosis* complex and *M. marinum* [60], and PE8 (F6B93_17700) and PPE15 (F6B93_17705) [36,61]. However, there are some potentially important differences too. For example, PE_PGRS47 (Rv2741), known to inhibit autophagy during *M. tuberculosis* infection, is absent from FSD4b-SM [62].

PE/PPE proteins that are involved in nutrient acquisition and stress resistance, such as PPE51 (F6B93_06205) and PE19 (F6B93_11045) are also present in FSD4b-SM with high levels of homology to their *M. tuberculosis* counterparts [56,63]. At least 29 of the putative FSD4b-SM PE/PPE proteins were confirmed to be expressed by proteomic analysis, including a LipY orthologue (F6B93_06345, LipY), which is involved in virulence in *M. tuberculosis* [64] (S8 Table). Overall, a large expansion of PE/PPE proteins, in particular those of the PE_PGRS and PPE-MPTR families, is seen in *M. spongiae*.

Unlike in *M. tuberculosis*, there are no IS element insertions associated with PE/PPE genes in FSD4b-SM, suggesting that the expansion of PE/PPE repertoire in this strain, relative to *M. tuberculosis*, has most likely occurred by gene duplication and homologous recombination [65,66]. Overall, the pattern of FSD4b-SM PE/PPE proteins follows that in other mycobacteria, with multiple, high-identity paralogues. The roles these PE/PPE proteins play in FSD4b-SM physiology remain to be discovered, but a role in protein export across the highly hydrophobic mycobacterial cell envelope is one candidate function [67].

Lipid biosynthesis pathways

The unique mycobacterial cell envelope is known to contain more than 50 classes of lipids and forms a barrier against many antibiotics and host immune defences. While mycolic acids make up approximately 30% of the outer layer of mycobacterial cells, other lipids such as the phthiocerol dimycocerosates (PDIMs) and phenolic glycolipids (PGLs) on the outer cell surface have important roles in pathogenicity and virulence [68]. Due to the importance of lipids in mycobacterial physiology and virulence, we undertook a genomic and lipidomic evaluation of lipid production in FSD4b-SM.

Lipid species that are conserved among all mycobacteria include the mycolic acids and mycocerosates. Multiple enzymes are involved in mycolic acid biosynthesis in mycobacteria and highly conserved orthologues of each, including those involved in methoxy and hydroxy mycolic acid production, were identified in the FSD4b-SM genome (S9 Table). Nearly all enzymes involved in mycolic acid biosynthesis were detected by our proteomic analysis, as were multiple mycolic acid species in our lipidomic analysis (Fig 3 and S9 and S10 Tables). Likewise, the key enzyme in mycocerosate biosynthesis, Mas (F6B93_07120 in FSD4b-SM), was also detected in FSD4b-SM by proteomics. Interestingly, FSD4b-SM Mas has higher amino acid similarity to *M. marinum* Mas than to *M. tuberculosis* Mas, including the presence of a conserved tryptophan within the enoylreductase (ER) domain [69], which leads to the production of 2 S configured methyl branches on mycocerosic acids, which have only previously been seen in *M. marinum* and *M. ulcerans* [70] (S11 Table).

Genes encoding enzymes that produce lipid molecules restricted to pathogenic mycobacteria were also found in the FSD4b-SM genome. These include genes for mannosyl- β -1-phosphomycoketides (*pks12*), which are key lipid antigens presented by human CD1c T-cells during *M. tuberculosis* infection, and genes involved in the *M. tuberculosis*-restricted acylated trehalose derivatives including di-, tri- and poly-acyl trehalose (DAT, TAT and PAT, respectively), albeit with some potential structural variation [71–73]. However, the putative DAT/TAT/PAT locus in FSD4b-SM is missing a critical FadD24 orthologue, which was found to be

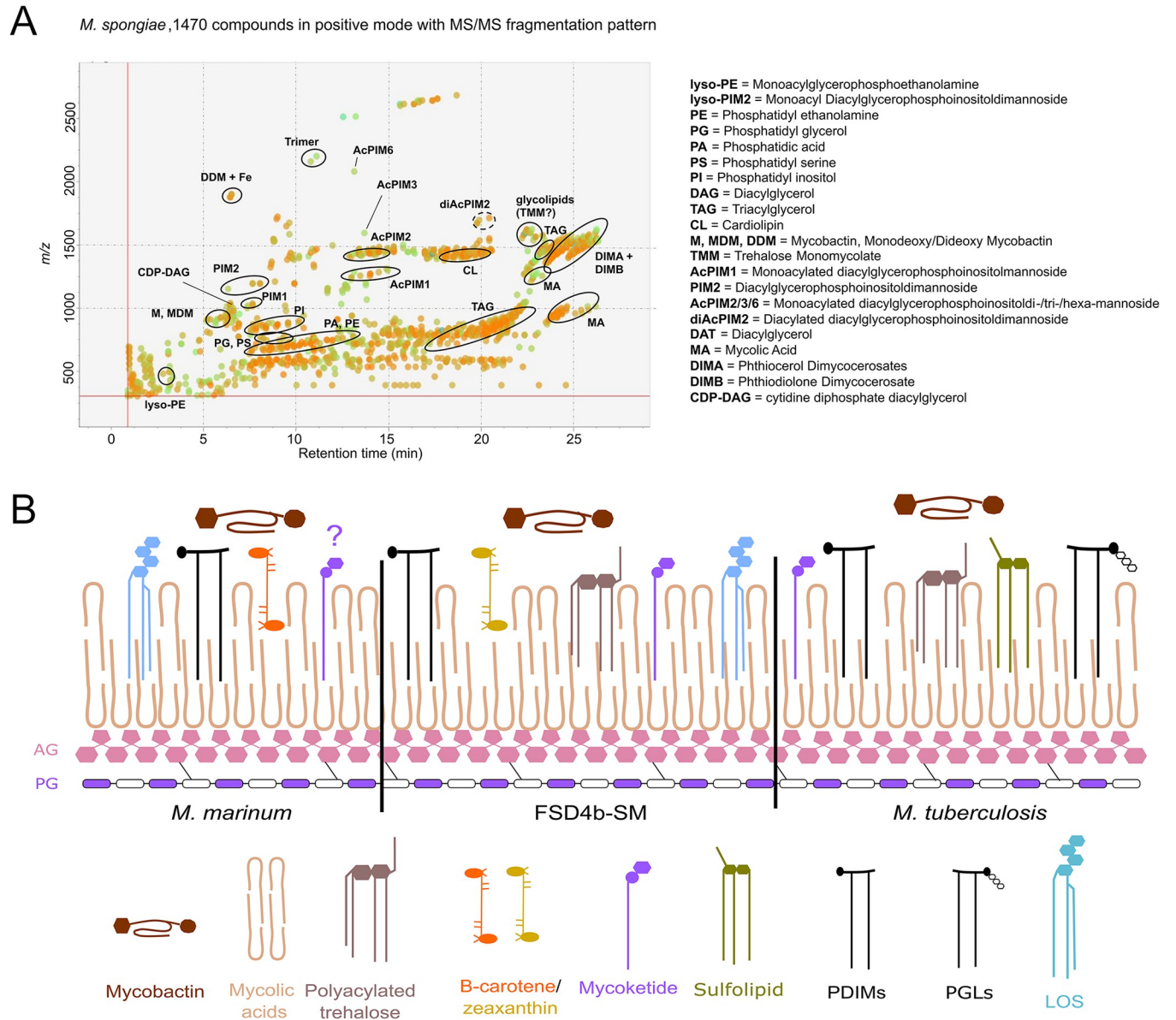


Fig 3. Lipidomic analysis of *M. spongiae*. A) MS/MS peak spot viewer of the *M. spongiae* extract in MS-DIAL showing retention time versus mass/charge ratio. Abundance (based on peak area) is shown as the colour of individual spots (blue = low, green = intermediate, orange = high abundance). Each lipid (sub) class is highlighted with a black circle. Note that not every spot within a circle belongs to the lipid (sub)class. B) Comparison of *M. marinum* and *M. tuberculosis* key membrane lipids with those predicted or detected from FSD4b-SM. The question mark above mycoketide for *M. marinum* indicates that the *M. marinum* genome contains a *pks12* orthologue, but mycoketides have not been detected from *M. marinum*. AG: arabinogalactan; PG: peptidoglycan; PDIMs: phthiocerol dimycocerosates; PGLs: phenolic glycolipids; LOS: lipooligosaccharide.

<https://doi.org/10.1371/journal.ppat.1012440.g003>

essential for both DAT and PAT formation in *M. tuberculosis* [74] (S4 Fig). DAT was not detected in our lipidomic analysis (S10 Table), although this absence may also be due to possible differences in the putative DAT enzymes in FSD4b-SM and *M. tuberculosis* (see S12 Table).

Genes for the production of the PDIMs were also identified, however, according to the biosynthetic logic (module and domain arrangement) of their producing polyketide synthases the FSD4b-SM enzymes should form unprecedented C9 D- and C11 L- configured phthiodiolone

glycols in FSD4b-SM, in contrast to the L and D configuration seen in *M. tuberculosis* and the L and L configuration in *M. marinum* (S5 Fig and S11 Table). However, these isomeric forms cannot be distinguished by our current lipidomic method. Genes for the formation of PGLs, which are thought to contribute to the hypervirulence of certain *M. tuberculosis* lineages are absent from FSD4b-SM and correspondingly no PGLs or their precursors were detected in our lipidomic analysis (S10 Table). Key genes for sulfolipid production appear to be only partially conserved in FSD4b-SM, suggesting that they are unlikely to be produced (S12 Table).

Unlike pathogen-specific lipids, the highly antigenic lipooligosaccharides (LOS) have been detected from several slow growing mycobacterial saprophytes and pathogens, including *M. canettii* [23], but not in *M. tuberculosis sensu stricto* [75]. Strains that make LOS contain a conserved genetic locus analogous to the DAT locus that contains two *pks* genes (*pks5* and *pks5.1*), FadD and Pap orthologues, as well as multiple glycosyltransferases (S12 Table) [76–78]. FSD4b-SM contains a LOS locus, which includes four *pks5* paralogues, compared to two in other species, suggesting a longer acyl chain may be added to the trehalose core (S7 Fig). In addition, FSD4b-SM also contains genes that appear to add a rhamnose to the acylated tetra-glucose core, suggesting that a previously unseen LOS is produced. FSD4b-SM also contains highly conserved genetic loci for the siderophore mycobactin and a *crt* locus, which is responsible for the production of the pigment beta-carotene in *M. marinum* [79] and *M. kansasii* [3]. Lipidomic analysis detected the presence of the related isoprenoid pigment zeaxanthin in FSD4b-SM extracts (S9 Table) and although zeaxanthin has not previously been detected from mycobacteria, it is known to be produced by many sea sponge-symbiotic bacteria [80,81], where the pigment is believed to act as an antioxidant and protect sponges from UV-induced damage [81]. These genomic, proteomic and metabolomic analyses of *M. spongiae* show that while its profile is distinct, it also has multiple features in common with *M. tuberculosis* as well as environmental opportunistic mycobacterial pathogens (Fig 3).

Assessment of FSD4b-SM pathogenicity and its potential as a *M. tuberculosis* vaccine strain

At present, *M. bovis* BCG is the only licensed anti-tuberculosis vaccine that provides good protection against childhood forms of tuberculosis, but it is less efficient in protecting against pulmonary tuberculosis in adolescents and adults [82]. A key reason for *M. bovis* BCG attenuation is the partial deletion of the ESX-1 locus and lack of major antigen ESAT-6 [83,84]. Early studies seeking to improve BCG by adding *M. tuberculosis* ESX-1 saw improved protection, but also increased virulence [84,85]. However, vaccine development using a rationally attenuated *M. tuberculosis* strain that still expresses ESAT-6 and CFP-10 showed increased protection relative to BCG, as did a recombinant BCG expressing the ESX-1 locus from the closely related *M. marinum* [42,86]. These studies are supported by a comprehensive analysis of recombinant BCG vaccines, which revealed that expression of ESX-1 derived effectors was an efficient way to improve BCG-induced immune responses [87]. As the FSD4b-SM ESX-1 locus is more closely related to that from *M. tuberculosis* than *M. marinum*, we sought to investigate if *M. bovis* BCG carrying ESX-1^{FSD4b-SM}, or alternatively *M. spongiae* FSD4b-SM itself, would provide improved protection compared with BCG against *M. tuberculosis* aerosol challenge in the murine infection model.

To construct a recombinant BCG strain expressing ESX-1^{FSD4b-SM} we used TAR cloning [88] to assemble the ESX-1 locus from eight overlapping PCR fragments in a yeast-*E. coli* shuttle vector and then subclone this region into the mycobacterial integrative vector pYUB412. Sequence analysis confirmed that the cloned region was identical to that from FSD4b-SM and this construct was integrated into *M. bovis* BCG at the phage L5 *attB* site. We then performed

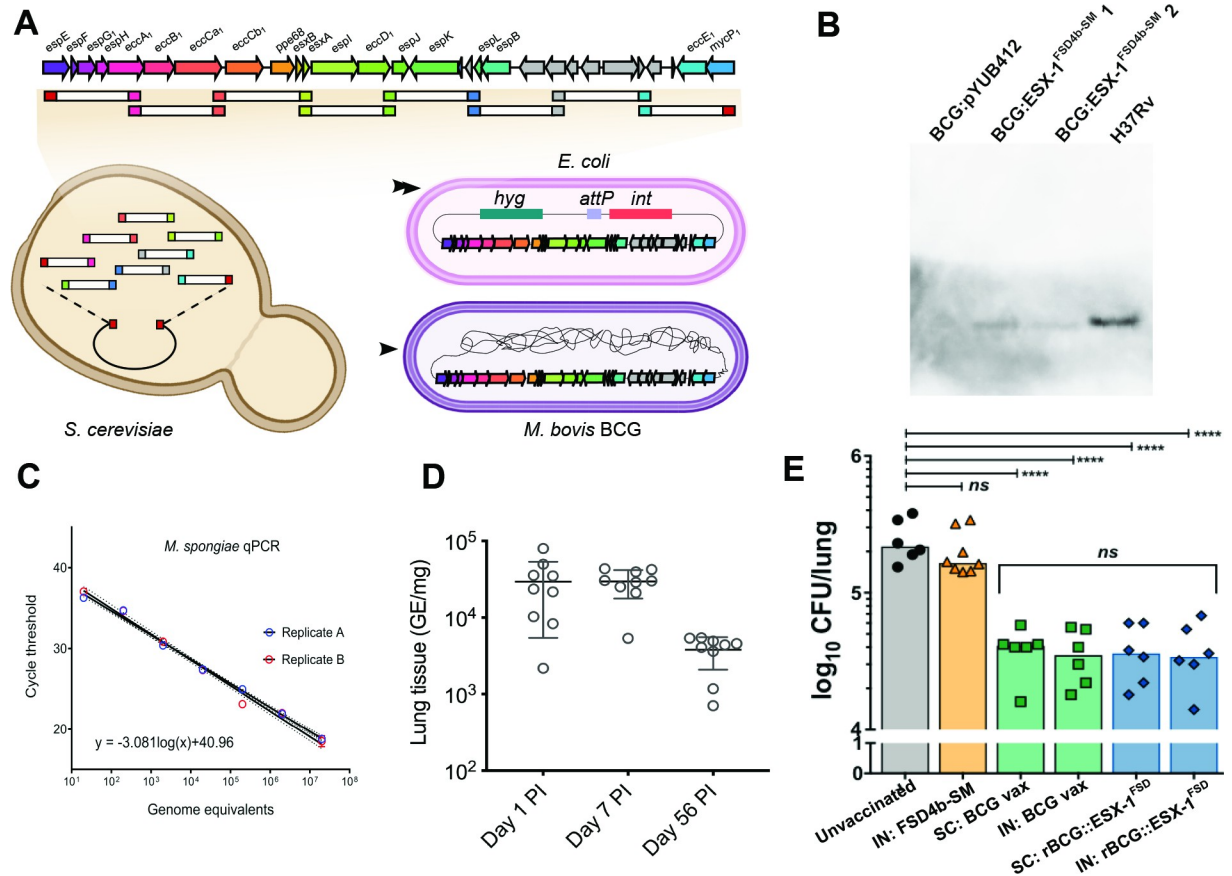


Fig 4. Construction of a recombinant *M. bovis* BCG with ESX-1FSD4b-SM and testing of its potential as an *M. tuberculosis* vaccine. A) The FSD4b-SM ESX-1 locus was assembled from eight overlapping PCR products in a yeast-*E. coli* shuttle vector in *Saccharomyces cerevisiae*, followed by transfer and sub-cloning of the ESX-1 locus into a mycobacterial integrative vector in *E. coli* and subsequent transfer and integration into the *M. bovis* BCG chromosome. B) Western blot with anti-CFP-10 antibody showing detection of CFP-10^{FSD4b-SM} from recombinant *M. bovis* BCG:ESX-1^{FSD4b-SM} and *M. tuberculosis* H37Rv CFP-10, but not from empty vector containing *M. bovis* BCG:pYUB412. BCG:ESX-1^{FSD4b-SM} 1 and 2 are two independent *M. bovis* BCG transformants. C) Establishment of a qPCR assay for detection of *M. spongiae* in mouse lung tissue. D) Mouse lung bacterial burden following intranasal inoculation of C57BL/6 wild type mice with live *M. spongiae*. Shown are mean and SD at days 1, 7 and 56 post-infection (PI). Three mice were sacrificed at each time point and qPCR reactions were performed in technical triplicates. E) Vaccination trial using *M. tuberculosis* H37Rv infectious aerosol challenge. Mice were vaccinated intranasally with *M. spongiae* FSD4b-SM or either intranasally or subcutaneously with *M. bovis* BCG (BCG vax), or recombinant *M. bovis* BCG expressing ESX-1 from *M. spongiae* (rBCG::ESX-1^{FSD}) and lungs were assayed for *M. tuberculosis* cells 4 weeks post challenge. Three mice were sacrificed in each group and *M. tuberculosis* counts were performed in duplicate. IN, intranasal; SC, subcutaneous.

<https://doi.org/10.1371/journal.ppat.1012440.g004>

western blot analysis using ESAT-6 and CFP-10 specific antibodies. Only CFP-10 was detected in culture supernatants, a phenomenon observed with other recombinant BCG:ESX-1 expression systems [42]. These experiments suggest that the ESX-1^{FSD4b-SM} was functional (Fig 4).

With a CFP-10-expressing recombinant BCG in hand, we next sought to investigate whether this strain would improve protection against *M. tuberculosis* challenge in a murine infection model. We also sought to investigate whether live FSD4b-SM could be used as a potential vaccine candidate, as has been seen for other environmental mycobacteria [89]. Due to the slow growth of FSD4b-SM, we developed a qPCR assay to monitor FSD4b-SM growth in mice, assaying lungs from three mice at each time point. We performed both subcutaneous and intra-nasal vaccination routes. Interestingly, we observed *M. spongiae* FSD4b-SM persisted in the mouse lung for at least 8-weeks post inoculation (Fig 4D). At autopsy, mice did not show any signs of pathology.

Infectious challenge experiments with aerosolised *M. tuberculosis* H37Rv showed no protection was offered by an intranasal dose of live *M. spongiae*, as recovered *M. tuberculosis* CFUs per lung were similar to unvaccinated control mice (Fig 4E). Recombinant *M. bovis* BCG:ESX-1^{FSD4b-SM} showed no further protection over the wild type *M. bovis* BCG vaccine, when delivered either subcutaneously or intranasally (Fig 4E). The CD4⁺ T cell response against immunogenic regions of EsxA is a good correlate of protection against *M. tuberculosis* in C57BL/6 (H-2^b) mice [85]. We therefore explored the cross recognition of an EsxA:1–20 immunogenic region of *M. bovis* BCG:ESX-1^{FSD4b-SM} by a T cell hybridoma specific to *M. tuberculosis* EsxA, restricted by major histocompatibility complex molecule-II, and representative of CD4⁺ effector T cells induced in vivo. A T cell hybridoma specific to Ag85A was used as a positive infection control (S8A–S8C Fig, top). Syngeneic DCs infected with recombinant *M. bovis* BCG:ESX-1^{FSD4b-SM} and co-cultured with NB11 T cell hybridomas [90] detected no cross recognition of EsxA from *M. bovis* BCG:ESX-1^{FSD4b-SM} (S8A–S8C Fig, middle), in accordance with the poor conservation of the immunodominant EsxA:1–20 epitope in *M. spongiae* FSD4b-SM (S8D Fig). However, as we also used an anti-EsxB T-cell hybridoma (XE12) that recognizes a 100% conserved EsxB region, restricted in the H-2^K haplotype [90], which was unable to detect *M. bovis* BCG:ESX-1^{FSD4b-SM}-infected DCs (S8A–S8C Fig, bottom), it is also possible that the EsxA and EsxB antigens from FSD4b-SM were not properly secreted by the recombinant BCG:ESX-1^{FSD4b-SM} strain under the infection conditions used in the experiment and thus not recognized. This may also explain why the use of this BCG:ESX-1^{FSD4b-SM} construct in vaccination experiments did not result in superior protection against *M. tuberculosis* challenge compared to BCG vaccination alone.

Conclusion

M. tuberculosis and the MTBC have co-existed with humans for millennia. Our knowledge of the evolutionary trajectory that transformed an environmental mycobacterium into a host-adapted mammalian pathogen is enriched every time a new mycobacterium related to the MTBC is discovered [2–4,91–94]. Genomic reconstructions indicate *M. tuberculosis* evolved from a common ancestor shared with several aquatic environment-associated mycobacteria, including *M. marinum*, *M. kansasii* and *M. lacus* [2,3]. Here we have shown that a mycobacterium isolated from a marine sponge, for which we have proposed the name *Mycobacterium spongiae* sp. nov. (“of the sponge”), occupies a phylogenetic position even closer to *M. tuberculosis* than these other mycobacteria, thus adding further support to the hypothesis that the MTBC might have evolved from a marine mycobacterium. It is also interesting to consider that while sponges are not like humans, human lungs are somewhat like sponges at both a gross mechano-anatomical level (they are both biological filters) and also perhaps more profoundly at a molecular evolutionary level, as exemplified by the discovery of a conserved TNF-driven fibrinogenic response to silica exposure in sponges, present also in mammals where it can lead to silicosis [95]. We don't yet know anything of the interaction between *M. spongiae*, the host sponge from which it was isolated, *Fascaplysinopsis reticulata*, and its holobiont. Such interactions will be interesting to observe.

The close genetic relationship between FSD4b-SM and *M. tuberculosis* and functional similarities assessed by proteomics and lipidomics prompted us to examine whether FSD4b-SM was pathogenic in a mouse model. Given that 8-weeks post-infection with live *M. spongiae* there was no observable pathology, this suggests that *M. spongiae* is non-pathogenic towards mice. Furthermore, our data show an inability of *M. spongiae* to grow at 37°C *in vitro* and this suggests that *M. spongiae* cannot also not grow and divide in the mouse model. Given the long generation time of *M. spongiae*, we used qPCR to detect *M. spongiae* DNA in mouse organs as

a surrogate for cell survival. While we observed a decrease in calculated genome equivalents over time (Fig 4D) we do not know at present whether this is due to extended DNA integrity or *M. spongiae* survival in a dormant state. Whatever the case, our data argue in favour of *M. spongiae* having low pathogenic potential in humans. Whether or not *M. spongiae* is a pathogen of aquatic animals remains to be seen and further experiments using models, such as zebrafish infection, are recommended.

In addition, we investigated whether components of *M. spongiae* could provide protection against *M. tuberculosis* challenge in a murine lung-infection model. While previous studies have shown that *M. bovis* BCG expressing *M. marinum* ESX-1 provided superior protection to BCG alone in mice [86], this was not the case for the ESX-1 locus from FSD4b-SM, despite the fact that the key ESX-1 antigens ESAT-6 and CFP-10 from FSD4b-SM are more closely related to *M. tuberculosis* than those from *M. marinum*, although we do not know how well the *M. spongiae* ESX-1 locus is expressed in *M. bovis* BCG during *in vivo* growth conditions in the mouse. Moreover, looking at the genomic comparison map of the ESX-1 loci from different mycobacterial species, we noted that the *pe35* gene upstream of *ppe68* is not present in *M. spongiae* (S2 Fig). In *M. tuberculosis*, this gene commonly plays an important role in effector function, as *pe35* transposon mutants show ESAT-6 secretion defects and lower virulence [96,97] although in such transposon mutants a possible effect of the transposon insertion on downstream effect might also be an explanation for this phenotype. However, the T cell hybridoma experiments were consistent with ESX-1 effector secretion defects and also help explain the poor vaccination outcome. Finally, the ESX-1 region of *M. spongiae* contains several extra genes compared to the ESX-1 loci of other mycobacteria (S2 Fig), whose potential impact on the functionality of the heterologous ESX-1 locus integrated into the BCG genome is unknown.

Overall, we describe a fascinating example of a slow growing, likely non-pathogenic mycobacterium we have designated *M. spongiae*, that is closely related to *M. tuberculosis*, sharing multiple genetic and functional similarities with the deadly human pathogen, while being adapted to the environmental conditions that prevail at 25 meters under the sea. It is presently unknown whether *M. spongiae* parasitises the sponge or only uses this ecological niche for its extracellular proliferation, but our findings strengthen the hypothesis that slow growing mycobacteria show an extraordinary capacity for adaptation to specific environments, a feature that has certainly also helped the ancestor of the tuberculosis-causing mycobacteria to adapt to mammalian hosts and conquer intracellular milieu.

Description of *Mycobacterium spongiae* sp. nov

***Mycobacterium spongiae* (spon'gi.ae. L. gen. n. *spongiae* of a sponge, the source of the type strain).** Short, compact acid-fast staining rods approx. 2 μ M in length and 0.4 μ M in diameter. Capable of aerobic growth on solid media typically used for culturing heterotrophic marine bacteria, although colony formation is scant. Does not grow on media typically used for mycobacterial growth such as Lowenstein-Jensen or egg-yolk-based agar media. In a simplified marine broth (artificial seawater with 0.5% peptone, 0.1% yeast extract) grows optimally at 28°C with an estimated doubling time of 64 days and reaches stationary phase after approximately three months. Type strain is unable to grow at 37°C. Closely related to the MTBC (*Mycobacterium tuberculosis* complex) on the basis of 16S rRNA, *hsp65* and *rpoB* gene sequences. The type strain has a 16S rRNA gene similarity value of 99.6% with *Mycobacterium tuberculosis*. The ANI (pairwise average nucleotide identity) between reference genomes is supportive of the status of a species adjacent to the MTBC. The relatively long branch length of the type strain within the *M. tuberculosis*-associated phylotype (MTBAP) cluster by

phylogenetic analysis based on amino acid sequence comparisons of 107 genes also supports distinct species status. Key *Mycobacterium tuberculosis* virulence factors are present, including intact ESX secretion systems and associated effectors. The genome size and number of coding DNA sequences of the type strain was 5,581,157 bp and 4458 genes (134 predicted pseudo-genes). There is a single rRNA locus. The average G+C percentage based on the genome was 65.56%.

The type strain is FSD4b-SM.

Materials and methods

Ethics statement

Animal procedures were reviewed and approved by The Walter and Eliza Hall Institute of Medical Research Animal Ethics Committee (ethics approval number 2017.016) and were conducted in accordance with the Prevention of Cruelty to Animals Act (1986) and the Australian National Health and Medical Research Council Code of Practice for the Care and Use of Animals for Scientific Purposes (1997).

Culture conditions

M. spongiae was grown in simplified marine broth (5 g/L peptone, 1 g/L yeast extract, 33 g/L artificial sea salt). For growth on plates, simplified marine broth was supplemented with 10 g/L bacteriological agar (Difco). Cultures were incubated at 28°C for 2 to 3 months without shaking. A list of strains and plasmids used in this study can be found in [S1 Table](#).

Growth curves

M. spongiae cultures were grown in 100 mL simplified marine broth at either 28°C or 37°C in biological triplicates. Cultures were started with a 1:100 dilution of a stationary phase *M. spongiae* culture. One milliliter samples were taken approximately every 2–3 weeks and optical density at 600nm was measured using an OD600 DiluPhotometer (Implen GmbH). Optical density readings are recorded in [S2 Table](#).

Electron microscopy

Transmission electron microscopy was performed by first washing *M. spongiae* FSD4b-SM cells from 3 month old cultures in PBS and pelleting by centrifugation at 10,000 x g for 5 min. Cells were then resuspended in fixation buffer (2.5% glutaraldehyde in 0.1 M sodium cacodylate) and incubated for 2 h at RT. Cells were then pelleted by centrifugation and washed twice with 0.1 M sodium cacodylate before post-fixation in 1% osmium tetroxide for 2 h at RT. Cell pellets were then washed in dH₂O, left overnight at 4°C in 0.3% uranyl acetate and then rinsed with dH₂O before being dehydrated using a graded series of acetone. Samples were then infiltrated and embedded with EPON resin. Sections (70–80 nm thick) were cut and stained with uranyl acetate and lead citrate before being viewed under a Phillips CM120 transmission electron microscope at 120 Kv.

Genome sequencing

High molecular weight genomic DNA was prepared using the DNeasy Blood and Tissue kit (QIAGEN), according to the manufacturer's instruction for Gram positive bacteria. A complete FSD4b-SM genome sequence was generated using a combination of PacBio and Illumina sequencing. For sequencing on the PacBio RSII, extracted DNA was prepared using the Template Prep Kit 1.0 (PacBio) and following adapter ligation DNA was size selected using a

BluePippin system (Sage Biosciences) with a 8 kb cut-off. Adapter-ligated, circularised DNA was loaded onto a single SMRT cell at 0.2 nM and sequence data were captured with a 6 h movie time. PacBio sequencing data was assembled using HGAP3, as implemented in the SMRT Portal (PacBio). The resulting genome was polished three times using Quiver (PacBio) before being error corrected with Illumina reads using Snippy v3.2 (<https://github.com/tseemann/snippy>). For Illumina sequencing, DNA libraries were created using the Nextera XT DNA preparation kit (Illumina) and whole genome sequencing was performed on the NextSeq platform (Illumina) with 2 x 150bp paired-end chemistry. A sequencing depth of >50× was targeted and the reads were used for error correcting the PacBio-assembled genome, as outlined above. The final 5,581,157 bp genome sequence was annotated using the NCBI Prokaryotic Genome Annotation Pipeline (PGAP) and assigned Genbank accession number CP046600.

Bioinformatics

Pairwise whole genome average nucleotide identity (ANI) was calculated using *fastANI* (<https://github.com/ParBLiSS/FastANI>) and *ANIClustermapper* (<https://github.com/moshi4/ANIClustermapper>) [98]. Core genome and ortholog comparisons were performed using *bcgTree* [12] and *Roary* [99]. Phylogenies were inferred using *iqtree* [100] using the the protein sequence alignment file output of *bcgTree*, with 1000 bootstrap replicates and the JTT model of amino acid substitution. A list of the mycobacterial genomes used for comparisons can be found in S3 Table. Individual protein homology searches were performed using BLAST, as implemented at NCBI (<https://www.ncbi.nlm.nih.gov/>), with multiple amino acid sequence alignments performed with ClustalW [101] and phylogenetic trees built using the Geneious tree builder (Geneious v9.1) (<https://www.geneious.com>). Analysis and alignment of ESX loci with *cblaster* [102] and *clinker* [103] was performed using the online *CompArative GENE Cluster Analysis* Toolbox (cagecat.bioinformatics.nl). Alignments of other loci were performed with *clinker* [103] at cagecat.bioinformatics.nl. PE/PPE proteins were identified through homology searching using BLAST and via annotation describing the protein as either a PE or PPE family member. All putative *M. spongiae* PE/PPE proteins were then aligned against known PE/PPE proteins and investigated for the presence of key domains/signature sequences according to criteria in [52]. Analysis of specialised metabolism was performed with anti-SMASH [14].

Extraction of and LC-MS analysis of mycobacterial lipids

Mycobacterial lipids were extracted and analysed as previously described [104]. In brief, cell pellets were extracted in 20 volumes of chloroform/methanol (2:1, v/v) followed by chloroform/methanol/water (1:2:0.8, v/v/v). Insoluble material was removed by centrifugation, extracts were dried under nitrogen and subjected to biphasic partitioning in 1-butanol and water (2:1, v/v). The organic phase was dried and lipids were resuspended in water-saturated 1-butanol. Lipid extracts were separated on an Agilent 1290 Infinity LC System (Agilent Technologies) using a Kinetex C 18 column (Phenomenex; 2.6 μm EVO C18 100Å) and eluted by using the following binary solvent system: mobile phase A (ACN:H₂O (60:40, v/v) with 10 mM ammonium formate) and mobile phase B (IPA:ACN (90:10, vol/vol), with 10 mM ammonium formate), with a 30 min gradient program. Eluted lipids were detected using a 6550 iFunnel QTOF LC/MS system (Agilent Technologies) with the same parameters as previously described [104]. Lipids were identified in positive ionization mode by accurate mass, fragmentation pattern, retention time and retention time order (different lipid groups and different

saturation levels show an elution time pattern and a relation to each other). MS-DIAL (Version 2.06; MS/MS data) was used for manual lipid annotation.

Proteomics

Samples for proteomics were prepared from FSD4B-SM cultures using the SP3 method [105]. Briefly, cells were lysed using buffer containing 50 mM HEPES, pH 8, 1% (wt/vol) SDS, 1% (vol/vol) Triton X-100, 1% (vol/vol) NP-40, 1% (vol/vol) Tween 20, 1% (wt/vol) deoxycholate, 5 mM EDTA, 50 mM NaCl, 1% (vol/vol) glycerol and beat beating for 6 x 30s in a Precellys 24 at speed 6.5. Insoluble material was removed by centrifugation at 20,000 x g for 10 min and the supernatant was transferred to a fresh tube. Protein concentration was measured using the BCA assay kit (Thermo Scientific) with bovine serum albumin as a standard. 10 µg protein was bound to SeraMag SpeedBeads Carboxylate-modified [E3] (Cytiva) and were digested overnight at 37°C with a 1:50 trypsin:protein ratio. Tryptic peptides were recovered and were cleaned up through SDB-RPS resin prior to submission for mass spectrometry.

The purified peptide samples were analysed via nano liquid chromatography coupled to tandem mass spectrometry (LC-MS/MS) at the University of Melbourne Mass Spectrometry and Proteomics Facility, using an Orbitrap Eclipse Tribrid Mass Spectrometer (Thermo Fisher Scientific, USA) equipped with a nano ESI interface coupled to an Ultimate 3000 nano HPLC (Thermo Fisher Scientific, USA). Peptides were separated using an Acclaim PepMap RSLC analytical column (C18, 100 Å, 75 µm × 50 cm, Thermo Fisher Scientific, USA) and Acclaim PepMap trap column (75 µm × 2 cm, C18, 100 Å). The enrichment column was injected with the tryptic peptides (3 µL) at an isocratic flow of 5 µL/min of 2% v/v CH₃CN containing 0.05% v/v aqueous trifluoroacetic acid for 6 min, applied before the enrichment column was switched in-line with the analytical column. The eluents were 0.1% v/v aqueous formic acid and 5% v/v dimethyl sulfoxide (DMSO) (solvent A) and 0.1% v/v formic acid and 5% DMSO in acetonitrile (solvent B). The gradient was at 300 nL min⁻¹ from (i) 0–6 min, 3% B; (ii) 6–35 min, 3–23% B; (iii) 35–45 min, 23–40% B; (iv) 45–50 min, 40–80% B; (v) 50–55 min, 80–80% B; (vi) 55–55.1 min, 80–3% B; (vii) 55.1–65 min, 3–3% B. The column oven was maintained at 50°C throughout the analysis. The Eclipse Orbitrap mass spectrometer was operated in the data-dependent mode, wherein full MS₁ spectra were acquired in a positive mode over the range of m/z 375–1500, with spray voltage at 1.9kV, source temperature at 275°C, MS₁ at 120,000 resolution and normalized AGC target of 100% and maximum ion injection time of 50 ms. The top 3 second method was used and selecting peptide ions with charge states of ≥ 2–7 and intensity thresholds of ≥ 5E4 were isolated for MS/MS. The isolation window was set at 1.6 m/z, and precursors were fragmented using higher energy C-trap dissociation (HCD) at a normalised collision energy of 30%, a resolution of 15,000, a normalized AGC target of 100% and automated IT time.

Protein fractionation and Western blotting of *M. spongiae*

M. spongiae FSD4B-SM liquid preculture of 25 ml was grown until an OD₆₀₀ of 0.15 was reached. At this point the complete culture was added to fresh simplified marine broth to a total volume of 100 ml. The cultures were incubated for 14 days in standing conditions at 30°C. After the 14 days of incubation, the culture had reached a density of 0.203 OD₆₀₀/ml. The culture was centrifuged in 2 x 50 ml falcon tubes at 5000 rpm for 10 minutes. The supernatant was taken and centrifuged again at 5000 rpm, after which the remaining supernatant (2 x 45ml) was collected and concentrated over a 3 kDa Amicon filter (Millipore). The residue was suspended in a volume of 900 µl. Pelleted cells after the first centrifugation step were washed once with PBS and resuspended in solubilisation buffer and boiled at 95°C for 15 minutes. An

equivalent of 0.3 OD₆₀₀ units of culture was loaded in each lane. *Mycobacterium tuberculosis* CDC1551 samples were loaded as a comparator. CDC1551 samples were taken from previously published protein fractions [106]. SDS-Page total protein content was imaged using standard Coomassie brilliant blue staining with Kaleidoscope molecular weight ladder (Biorad). Antibodies tested to visualize *M. spongiae* proteins included Anti-PGRS 7C4.1F7 [107] (Clone 7C4.1F7 was a kind gift from Michael J. Brennan, USA); polyclonal anti-SigA (Kind gift from I. Rosenkrands, Denmark); monoclonal ESAT-6 (hyb76-8) [108]; anti-GroEL2 antibody CS-44 (Kind gift from J. Belisle, Colorado State University, Fort Collins, CO); Rabbit polyclonal anti-EsxN (rMTb9.9A) [109].

TAR cloning of the *M. spongiae* ESX-1 region

To design primers for amplification of the FSD4b-SM ESX-1 locus, the region was divided into 8 theoretical fragments of approximately equivalent length. Primers were then designed so that each PCR fragment would overlap by at least 30bp of DNA (see S4 Table for primer sequences). DNA fragments were amplified using Phusion DNA polymerase (NEB) in reactions containing 10% DMSO and using GC buffer. The program for amplification was: 1 cycle of 95°C for 5' then 30 cycles of 95°C for 10s, 72°C for 2 min 30s followed by a final extension at 72°C for 7 minutes. PCR products were cleaned up using AMPure XP beads (Beckman Coulter). The GeneArt High-Order Genetic Assembly kit (Thermo Fisher Scientific) was used to assemble the PCR products into the vector pYES1L by transformation into *Saccharomyces cerevisiae* MaV203 cells. The manufacturers protocols were followed for all steps. Recovered pYES1L:ESX-1^{FSD4b-SM} DNA was sequenced using Illumina sequencing to confirm the correct sequence. The 33.3 kb ESX-1^{FSD4b-SM} region from pYES1L:ESX-1^{FSD4b-SM} was then subcloned by digestion with *Sbf*I and gel extraction followed by ligation into the mycobacteria-*E. coli* shuttle vector pYUB412 that had been digested with *Sbf*I. The resulting ligation mixture was transformed by electroporation into *E. coli* DH10B and colonies were screened by PCR for the presence of the ESX-1^{FSD4b-SM} region. Cloning of the full-length ESX-1^{FSD4b-SM} region was confirmed by restriction digestion. The resulting pYUB412:ESX-1^{FSD4b-SM} plasmid was transformed into *M. bovis* BCG by electroporation according to standard protocols [110].

qPCR to estimate *M. spongiae* concentration in mouse tissues

A standard TaqMan assay was designed for quantitative, specific detection of *M. spongiae* in mouse tissue specimens. A PCR amplicon was designed spanning a 64bp region of F6B93_05840, a CDS encoding a hypothetical aquaporin protein. The primer sequences were: FSD4b_05840-F 5'- ACGTCAGGCTTGATGCTCTC-3' and FSD4b_05840-R 5'- GCGCTAC-CAGATAGACCCAG-3'. The internal probe sequence was FSD4b_05840-P: 5'- [6FAM] CGGGTTTTTCTCGTGGAAAGT[BHQ1] -3'. The qPCR was performed as described [111] using 2x SensiFast mastermix (Bioline) with primers and probes to a final concentration in 25uL reaction volume of 0.32uM (primers) and 0.16uM (probe) respectively. Each reaction included internal positive control reagents and DNA template with 2uL volume of sample template DNA. PCR cycles included 1x 95oC 5min followed by 45x 95oC for 10s and then 60°C for 20s. PCR was performed in a LC480 Lightcycler (Roche). A standard curve was prepared using 10-fold serial, replicate dilutions of *M. spongiae* purified genomic DNA. Genomic DNA concentrations were measured using fluorimetry (Qubit, ThermoFisher).

Mouse vaccination and infectious challenge

Wild-type C57BL/6 mice were bred and maintained at The Walter and Eliza Hall Institute of Medical Research Animal Facility. Intranasal and subcutaneous vaccinations were performed

in 50 μ L volumes in PBS containing either 10^4 CFU of live *M. spongiae*, or 5×10^4 CFU of the WT or BCG::ESX-1^{FSD4b-SM} modified *M. bovis* BCG strains (the same dose was given for both intranasal and subcutaneous vaccination).

For *M. tuberculosis* infectious challenge, mice were infected with 50–200 colony-forming units (CFU) of *M. tuberculosis* H37Rv by aerosol using a whole-body Inhalation Exposure System (Glas-Col) four months after vaccination, as described [112]. A bacterial suspension containing $\sim 2.5 \times 10^8$ CFU in 6 mL was aerosolized over a period of 45 min. Mice were euthanized four weeks post-infection by CO₂ asphyxiation. Spleens and the right lung lobes were aseptically harvested and homogenized with steel beads in PBS+0.05% Tween-80 using a Bullet Blender (Next Advance) at setting #6 for 3 min (spleens) or #8 for 5 min (lungs). Tissue homogenates for counting *M. tuberculosis* were serially diluted and spread on 7H11 agar plates (BD Biosciences) supplemented with 0.5% glycerol and 10% (v/v) oleic-albumin-dextrose-catalase supplements (50 g/l BSA, 20 g/l dextrose, 0.04 g/l catalase and 0.5 g/l oleic acid [Sigma-Aldrich]). Plates were incubated at 37°C for 3 weeks before counting. *M. spongiae* DNA was extracted from mouse tissues using DNAeasy Blood and Tissue kit (Qiagen). The numbers of mice used in each individual experiment were calculated to permit detection of at least a two- to four-fold difference in bacterial loads between groups with 95% (two-sided) confidence and a power of 80%, based on prior experience.

For all experiments, mice were weighed daily and humane weight-based endpoints were set as weight loss >10% for more than 3 days. No mice were euthanized under these weight-based endpoints, and no mice lost >15% weight on any day.

Supporting information

S1 Table. Strains and plasmids used in this study.

(XLSX)

S2 Table. OD₆₀₀ measurements for *M. spongiae* growth curve at 28°C and 37°C.

(XLSX)

S3 Table. Genomes used for phylogenetic analysis.

(XLSX)

S4 Table. Primers used for construction of pYES1L:ESX-1^{FSD4b-SM}.

(XLSX)

S5 Table. *M. tuberculosis* virulence factors identified in *M. spongiae* genome.

(XLSX)

S6 Table. DNA methylation patterns identified in the *M. spongiae* genome.

(XLSX)

S7 Table. Orthologues of *M. tuberculosis* ESX system proteins in *M. spongiae*.

(XLSX)

S8 Table. PE/PPE proteins identified in FSD4b-SM and *M. tuberculosis* PE/PPE orthologues.

(XLSX)

S9 Table. Orthologues of mycolic acid biosynthesis proteins in *M. spongiae*.

(XLSX)

S10 Table. Summary of key lipid species identified in *M. spongiae*.

(XLSX)

S11 Table. Orthologues involved in the biosynthesis of phthiocerol dimycocerosates, phenolic glycolipids, and p-hydroxybenzoic acids.

(XLSX)

S12 Table. Orthologues of proteins involved in biosynthesis of trehalose and related compounds.

(XLSX)

S13 Table. Orthologues of proteins involved in the biosynthesis of phospholipids, isoprenoids and related compounds.

(XLSX)

S1 Fig. Analysis of energetics from *M. spongiae* genome. Blue bars indicate conservation of a particular system with other mycobacteria, while red bars indicate absence of a particular system.

(TIF)

S2 Fig. Alignment of ESX-1 and ESX-5 loci from *M. spongiae* FD4b-SM and other related mycobacteria. Pairwise percentage identity between encoded proteins is shown in white text, locus tags are written in black. Common gene names for each the Esx proteins are coloured according to the gene on which they are encoded.

(TIF)

S3 Fig. Exuberant expression of PE_PGRS proteins in *M. spongiae*. (A) SDS-PAGE, Coomassie brilliant blue stained gel, showing protein loading for *M. spongiae* and *M. tuberculosis*. (B). Western blot analysis using anti-PE_PGRS antibody against *M. spongiae* and *M. tuberculosis*. WCL = Whole Cell Lysate. CF = Culture Filtrate.

(TIF)

S4 Fig. Alignment of putative *pks3/4* locus in *M. spongiae* with that from *M. tuberculosis*. PKS domains are indicated underneath each putative PKS protein. Note the absence of a *fadD24* orthologue in *M. spongiae*.

(TIF)

S5 Fig. Predicted phthiodiolone diphthiocerante biosynthetic pathway in FSD4b-SM and comparison to phthiocerol dimycocerosate biosynthetic pathway in *M. tuberculosis*.

(TIF)

S6 Fig. Alignment of *pks7-11* region in *M. tuberculosis* with that from *M. spongiae*.

(TIF)

S7 Fig. Alignment of putative LOS locus in *M. spongiae* with those from other mycobacteria. Note the four *pks* genes in the *M. spongiae* genome.

(TIF)

S8 Fig. Assessment of recombinant *M. bovis* BCG FSD4b-SM Esx-1 protein effector T cell stimulation. (A–D) Measurement of IL-2 production by T cell hybridomas specific for epitopes from *M. tuberculosis* H37Rv antigens Ag85A, EsxA, and EsxB, after co-culture with DCs: (A) infected with various *M. bovis* BCG recombinant ESX-1 strains, (B) infected with WT *M. tuberculosis* H37Rv or an ESX-1 deletion mutant, or (C) loaded with Ag85A, EsxA, and EsxB peptides encompassing the immunodominant epitopes or control peptide. Shown are concentrations of IL-2 in the co-culture supernatants at 24hr after T cell addition. Error bars are mean and SD of triplicate experiments. (D) Amino acid sequence alignments of *M. spongiae* FSD4b-SM Ag85A, EsxA and EsxB with *M. tuberculosis* H37Rv orthologs, showing

conservation and differences with the T cell epitopes.
(TIF)

Acknowledgments

The authors wish to acknowledge the help of staff of the Mass Spectrometry facility at the Bio21 Institute, University of Melbourne.

Author Contributions

Conceptualization: Sacha J. Pidot, Stephan Klatt, Louis S. Ates, Timothy P. Stinear.

Data curation: Sacha J. Pidot, Stephan Klatt, Louis S. Ates, Torsten Seemann, Michael D. Stutz.

Formal analysis: Sacha J. Pidot, Stephan Klatt, Louis S. Ates, Wafa Frigui, Fadel Sayes, Laleh Majlessi, Hiroshi Izumi, Ian R. Monk, Jessica L. Porter, Vicki Bennett-Wood, Torsten Seemann, Ashley Otter, George Tairaroa, Nicholas West, Nicholas J. Tobias, Michael D. Stutz.

Funding acquisition: Sacha J. Pidot, Marc Pellegrini, Malcolm McConville, Timothy P. Stinear.

Investigation: Sacha J. Pidot, Stephan Klatt, Louis S. Ates, Wafa Frigui, Fadel Sayes, Laleh Majlessi, Hiroshi Izumi, Ian R. Monk, Jessica L. Porter, Vicki Bennett-Wood, Ashley Otter, George Tairaroa, Gregory M. Cook, Nicholas West, Nicholas J. Tobias, Michael D. Stutz, Marc Pellegrini, Roland Brosch, Timothy P. Stinear.

Methodology: Sacha J. Pidot, Stephan Klatt, Ian R. Monk, Jessica L. Porter.

Project administration: Sacha J. Pidot.

Resources: John A. Fuerst, Marc Pellegrini, Malcolm McConville, Roland Brosch, Timothy P. Stinear.

Supervision: Gregory M. Cook, John A. Fuerst, Marc Pellegrini, Malcolm McConville, Roland Brosch, Timothy P. Stinear.

Validation: Michael D. Stutz.

Writing – original draft: Sacha J. Pidot, Stephan Klatt, Louis S. Ates, Roland Brosch, Timothy P. Stinear.

Writing – review & editing: Sacha J. Pidot, Stephan Klatt, Gregory M. Cook, John A. Fuerst, Roland Brosch, Timothy P. Stinear.

References

1. WHO. Global Tuberculosis Report 2022. Geneva: World Health Organisation; 2022.
2. Stinear TP, Seemann T, Harrison PF, Jenkin GA, Davies JK, Johnson PD, et al. Insights from the complete genome sequence of *Mycobacterium marinum* on the evolution of *Mycobacterium tuberculosis*. *Genome Res.* 2008 May; 18(5):729–41. <https://doi.org/10.1101/gr.075069.107> PMID: 18403782
3. Wang J, McIntosh F, Radomski N, Dewar K, Simeone R, Enninga J, et al. Insights on the emergence of *Mycobacterium tuberculosis* from the analysis of *Mycobacterium kansasii*. *Genome Biol Evol.* 2015 Feb 25; 7(3):856–70. <https://doi.org/10.1093/gbe/evv035> PMID: 25716827
4. Sapriel G, Brosch R. Shared pathogenomic patterns characterize a new phylotype, revealing transition toward host-adaptation long before speciation of *Mycobacterium tuberculosis*. *Genome Biol Evol.* 2019 Aug 1; 11(8):2420–38. <https://doi.org/10.1093/gbe/evz162> PMID: 31368488

5. Thomas T, Moitinho-Silva L, Lurgi M, Bjork JR, Easson C, Astudillo-Garcia C, et al. Diversity, structure and convergent evolution of the global sponge microbiome. *Nat Commun.* 2016 Jun 16; 7:11870. <https://doi.org/10.1038/ncomms11870> PMID: 27306690
6. Moitinho-Silva L, Nielsen S, Amir A, Gonzalez A, Ackermann GL, Cerrano C, et al. The sponge microbiome project. *Gigascience.* 2017 Oct; 6(10):1–7. <https://doi.org/10.1093/gigascience/gix077> PMID: 29020741
7. Busch K, Slaby BM, Bach W, Boetius A, Clefsen I, Colaço A, et al. Biodiversity, environmental drivers, and sustainability of the global deep-sea sponge microbiome. *Nat Commun.* 2022 Sep 2; 13(1):5160. <https://doi.org/10.1038/s41467-022-32684-4> PMID: 36056000
8. Izumi H, Gauthier ME, Degnan BM, Ng YK, Hewavitharana AK, Shaw PN, et al. Diversity of Mycobacterium species from marine sponges and their sensitivity to antagonism by sponge-derived rifamycin-synthesizing actinobacterium in the genus *Salinispora*. *FEMS Microbiol Lett.* 2010 Dec; 313(1):33–40. <https://doi.org/10.1111/j.1574-6968.2010.02118.x> PMID: 20883497
9. Cole ST, Brosch R, Parkhill J, Garnier T, Churcher C, Harris D, et al. Deciphering the biology of Mycobacterium tuberculosis from the complete genome sequence. *Nature.* 1998 Jun 11; 393(6685):537–44. <https://doi.org/10.1038/31159> PMID: 9634230
10. Camus JC, Pryor MJ, Medigue C, Cole ST. Re-annotation of the genome sequence of Mycobacterium tuberculosis H37Rv. *Microbiology.* 2002 Oct; 148(Pt 10):2967–73. <https://doi.org/10.1099/00221287-148-10-2967> PMID: 12368430
11. Veyrier F, Pletzer D, Turenne C, Behr MA. Phylogenetic detection of horizontal gene transfer during the step-wise genesis of Mycobacterium tuberculosis. *BMC Evol Biol.* 2009 Aug 10; 9:196. <https://doi.org/10.1186/1471-2148-9-196> PMID: 19664275
12. Ankenbrand MJ, Keller A. bcgTree: automatized phylogenetic tree building from bacterial core genomes. *Genome.* 2016 Oct; 59(10):783–91. <https://doi.org/10.1139/gen-2015-0175> PMID: 27603265
13. Meier JL, Burkart MD. The chemical biology of modular biosynthetic enzymes. *Chem Soc Rev.* 2009 Jul; 38(7):2012–45. <https://doi.org/10.1039/b805115c> PMID: 19551180
14. Blin K, Shaw S, Kloosterman AM, Charlop-Powers Z, van Wezel GP, Medema MH, et al. AntiSMASH 6.0: improving cluster detection and comparison capabilities. *Nucl Acids Res.* 2021 Jul 2; 49(W1):W29–35. <https://doi.org/10.1093/nar/gkab335> PMID: 33978755
15. Harris NC, Sato M, Herman NA, Twigg F, Cai W, Liu J, et al. Biosynthesis of isonitrile lipopeptides by conserved nonribosomal peptide synthetase gene clusters in Actinobacteria. *Proc Natl Acad Sci U S A.* 2017 Jul; 114(27):7025–30. <https://doi.org/10.1073/pnas.1705016114> PMID: 28634299
16. Martins TP, Rouger C, Glasser NR, Freitas S, Fraissinette NB de, Balskus EP, et al. Chemistry, bioactivity and biosynthesis of cyanobacterial alkylresorcinols. *Nat Prod Rep.* 2019 Oct 16; 36(10):1437–61. <https://doi.org/10.1039/c8np00080h> PMID: 30702733
17. Zhang F, Xie JP. Mammalian cell entry gene family of Mycobacterium tuberculosis. *Mol Cell Biochem.* 2011 Jun; 352(1–2):1–10. <https://doi.org/10.1007/s11010-011-0733-5> PMID: 21258845
18. Gonzalo-Asensio J, Malaga W, Pawlik A, Astarie-Dequeker C, Passemar C, Moreau F, et al. Evolutionary history of tuberculosis shaped by conserved mutations in the PhoPR virulence regulator. *Proc Natl Acad Sci USA.* 2014 Aug 5; 111(31):11491–6. <https://doi.org/10.1073/pnas.1406693111> PMID: 25049399
19. Malaga W, Payros D, Meunier E, Frigui W, Sayes F, Pawlik A, et al. Natural mutations in the sensor kinase of the PhoPR two-component regulatory system modulate virulence of ancestor-like tuberculosis bacilli. *PLoS Pathog.* 2023 Jul 14; 19(7):e1011437. <https://doi.org/10.1371/journal.ppat.1011437> PMID: 37450466
20. Miotto P, Sorrentino R, De Giorgi S, Provvedi R, Cirillo DM, Manganelli R. Transcriptional regulation and drug resistance in Mycobacterium tuberculosis. *Front Cell Infect Microbiol.* 2022; 12:990312. <https://doi.org/10.3389/fcimb.2022.990312> PMID: 36118045
21. Converse PJ, Karakousis PC, Klinkenberg LG, Kesavan AK, Ly LH, Allen SS, et al. Role of the dosR-dosS Two-Component Regulatory System in Mycobacterium tuberculosis Virulence in Three Animal Models. *Infect Immun.* 2009 Mar; 77(3):1230–7. <https://doi.org/10.1128/IAI.01117-08> PMID: 19103767
22. Kumar A, Toledo JC, Patel RP, Lancaster JR Jr, Steyn AJ. Mycobacterium tuberculosis DosS is a redox sensor and DosT is a hypoxia sensor. *Proc Natl Acad Sci U S A.* 2007 Jul 10; 104(28):11568–73. <https://doi.org/10.1073/pnas.0705054104> PMID: 17609369
23. Boritsch EC, Frigui W, Cascioferro A, Malaga W, Etienne G, Laval F, et al. pks5-recombination-mediated surface remodelling in Mycobacterium tuberculosis emergence. *Nat Microbiol.* 2016 Jan 27; 1:15019. <https://doi.org/10.1038/nmicrobiol.2015.19> PMID: 27571976

24. Danilchanka O, Sun J, Pavlenok M, Maueröder C, Speer A, Siroy A, et al. An outer membrane channel protein of *Mycobacterium tuberculosis* with exotoxin activity. *Proc Natl Acad Sci USA*. 2014 May 6; 111(18):6750–5. <https://doi.org/10.1073/pnas.1400136111> PMID: 24753609
25. Speer A, Sun J, Danilchanka O, Meikle V, Rowland JL, Walter K, et al. Surface hydrolysis of sphingomyelin by the outer membrane protein Rv0888 supports replication of *Mycobacterium tuberculosis* in macrophages. *Mol Microbiol*. 2015; 97(5):881–97. <https://doi.org/10.1111/mmi.13073> PMID: 26036301
26. Gordon SV, Brosch R, Billault A, Garnier T, Eiglmeier K, Cole ST. Identification of variable regions in the genomes of tubercle bacilli using bacterial artificial chromosome arrays. *Mol Microbiol*. 1999 May; 32(3):643–55. <https://doi.org/10.1046/j.1365-2958.1999.01383.x> PMID: 10320585
27. Ainsa JA, Perez E, Pelicic V, Berthet FX, Gicquel B, Martin C. Aminoglycoside 2'-N-acetyltransferase genes are universally present in mycobacteria: characterization of the *aac(2')-Ic* gene from *Mycobacterium tuberculosis* and the *aac(2')-Id* gene from *Mycobacterium smegmatis*. *Mol Microbiol*. 1997 Apr; 24(2):431–41. <https://doi.org/10.1046/j.1365-2958.1997.3471717.x> PMID: 9159528
28. Verma AK, Chatterji D. Dual role of MsRbpA: transcription activation and rescue of transcription from the inhibitory effect of rifampicin. *Microbiology*. 2014; 160(9):2018–29. <https://doi.org/10.1099/mic.0.079186-0> PMID: 24987104
29. Chu H, Hu Y, Zhang B, Sun Z, Zhu B. DNA Methyltransferase HsdM Induce Drug Resistance on *Mycobacterium tuberculosis* via Multiple Effects. *Antibiotics*. 2021 Dec; 10(12):1544. <https://doi.org/10.3390/antibiotics10121544> PMID: 34943756
30. He H, Bretl DJ, Penoske RM, Anderson DM, Zahrt TC. Components of the Rv0081-Rv0088 Locus, Which Encodes a Predicted Formate Hydrogenlyase Complex, Are Coregulated by Rv0081, MprA, and DosR in *Mycobacterium tuberculosis*. *J Bact*. 2011 Sep 13; 193(19):5105–18. <https://doi.org/10.1128/JB.05562-11> PMID: 21821774
31. Berney M, Greening C, Hards K, Collins D, Cook GM. Three different [NiFe] hydrogenases confer metabolic flexibility in the obligate aerobe *Mycobacterium smegmatis*. *Env Microbiol*. 2014; 16(1):318–30. <https://doi.org/10.1111/1462-2920.12320> PMID: 24536093
32. Grinter R, Kropp A, Venugopal H, Senger M, Badley J, Cabotaje PR, et al. Structural basis for bacterial energy extraction from atmospheric hydrogen. *Nature*. 2023 Mar; 615(7952):541–7. <https://doi.org/10.1038/s41586-023-05781-7> PMID: 36890228
33. Lappan R, Shelley G, Islam ZF, Leung PM, Lockwood S, Nauer PA, et al. Molecular hydrogen in seawater supports growth of diverse marine bacteria. *Nat Microbiol*. 2023 Apr; 8(4):581–95. <https://doi.org/10.1038/s41564-023-01322-0> PMID: 36747116
34. Groschel MI, Sayes F, Simeone R, Majlessi L, Brosch R. ESX secretion systems: mycobacterial evolution to counter host immunity. *Nat Rev Microbiol*. 2016 Nov; 14(11):677–91. <https://doi.org/10.1038/nrmicro.2016.131> PMID: 27665717
35. Tufariello JM, Chapman JR, Kerantzas CA, Wong KW, Vilcheze C, Jones CM, et al. Separable roles for *Mycobacterium tuberculosis* ESX-3 effectors in iron acquisition and virulence. *Proc Natl Acad Sci U S A*. 2016 Jan 19; 113(3):E348–57. <https://doi.org/10.1073/pnas.1523321113> PMID: 26729876
36. Ates LS, Ummels R, Commandeur S, van de Weerd R, Sparrius M, Weerdenburg E, et al. Essential role of the *esx-5* secretion system in outer membrane permeability of pathogenic mycobacteria. *PLoS Genet*. 2015 May; 11(5):e1005190. <https://doi.org/10.1371/journal.pgen.1005190> PMID: 25938982
37. Ramakrishnan L, Federspiel NA, Falkow S. Granuloma-specific expression of mycobacterium virulence proteins from the glycine-rich PE-PGRS family. *Science*. 2000 May 26; 288(5470):1436–9. <https://doi.org/10.1126/science.288.5470.1436> PMID: 10827956
38. Singh VK, Berry L, Bernut A, Singh S, Carrère-Kremer S, Viljoen A, et al. A unique PE_PGRS protein inhibiting host cell cytosolic defenses and sustaining full virulence of *Mycobacterium marinum* in multiple hosts. *Cell Microbiol*. 2016; 18(11):1489–507. <https://doi.org/10.1111/cmi.12606> PMID: 27120981
39. Damen MPM, Meijers AS, Keizer EM, Piersma SR, Jiménez CR, Kuijl CP, et al. The ESX-1 substrate PPE68 has a key function in ESX-1-mediated secretion in *Mycobacterium marinum*. *mBio*. 2022 Nov 21; 13(6):e02819–22. <https://doi.org/10.1128/mbio.02819-22> PMID: 36409073
40. Gijsbers A, Eymery M, Gao Y, Menart I, Vinciauskaite V, Siliqi D, et al. The crystal structure of the EspB-EspK virulence factor-chaperone complex suggests an additional type VII secretion mechanism in *Mycobacterium tuberculosis*. *J Biol Chem*. 2023; 299(1):102761. <https://doi.org/10.1016/j.jbc.2022.102761> PMID: 36463964
41. Zhang M, Chen JM, Sala C, Rybniker J, Dhar N, Cole ST. Espl regulates the ESX-1 secretion system in response to ATP levels in *Mycobacterium tuberculosis*. *Mol Microbiol*. 2014; 93(5):1057–65. <https://doi.org/10.1111/mmi.12718> PMID: 25039394
42. Aguilo N, Gonzalo-Asensio J, Alvarez-Arguedas S, Marinova D, Gomez AB, Uranga S, et al. Reactogenicity to major tuberculosis antigens absent in BCG is linked to improved protection against

- Mycobacterium tuberculosis. Nat Commun. 2017 Jul 14; 8(1):16085. <https://doi.org/10.1038/ncomms16085> PMID: 28706226
43. Di Luca M, Bottai D, Batoni G, Orgeur M, Alicino A, Counoupas C, et al. The ESX-5 associated eccB5-eccC5 locus is essential for Mycobacterium tuberculosis viability. PLoS One. 2012 Dec 17; 7(12):e52059.
 44. Saelens JW, Sweeney MI, Viswanathan G, Xet-Mull AM, Smith KLJ, Sisk DM, et al. An ancestral mycobacterial effector promotes dissemination of infection. Cell. 2022 Nov 23; 185(24):4507–4525. e18. <https://doi.org/10.1016/j.cell.2022.10.019> PMID: 36356582
 45. Ates LS, Houben ENG, Bitter W. Type VII secretion: A highly versatile secretion system. Microbiol Spect. 2016; 4(1):10.1128/microbiolspec.vmbf-0011–2015. <https://doi.org/10.1128/microbiolspec.VMBF-0011-2015> PMID: 26999398
 46. Fishbein S, van Wyk N, Warren RM, Sampson SL. Phylogeny to function: PE/PPE protein evolution and impact on Mycobacterium tuberculosis pathogenicity. Mol Microbiol. 2015 Jun; 96(5):901–16. <https://doi.org/10.1111/mmi.12981> PMID: 25727695
 47. Brennan MJ. The enigmatic PE/PPE multigene family of mycobacteria and tuberculosis vaccination. Infect Immun. 2017; 85(6):e00969–16.
 48. Mitra A, Speer A, Lin K, Ehrh S, Niederweis M. PPE Surface Proteins Are Required for Heme Utilization by Mycobacterium tuberculosis. mBio. 2017; 8(1):e01720–16. <https://doi.org/10.1128/mBio.01720-16> PMID: 28119467
 49. DeJesus MA, Gerrick ER, Xu W, Park SW, Long JE, Boutte CC, et al. Comprehensive essentiality analysis of the Mycobacterium tuberculosis genome via saturating transposon mutagenesis. mBio. 2017; 8(1):e02133–16. <https://doi.org/10.1128/mBio.02133-16> PMID: 28096490
 50. Sassetti CM, Boyd DH, Rubin EJ. Comprehensive identification of conditionally essential genes in mycobacteria. Proc Natl Acad Sci USA. 2001 Oct 23; 98(22):12712–7. <https://doi.org/10.1073/pnas.231275498> PMID: 11606763
 51. Gey van Pittius NC, Sampson SL, Lee H, Kim Y, van Helden PD, Warren RM. Evolution and expansion of the Mycobacterium tuberculosis PE and PPE multigene families and their association with the duplication of the ESAT-6 (esx) gene cluster regions. BMC Evol Biol. 2006 Nov 15; 6(1):95. <https://doi.org/10.1186/1471-2148-6-95> PMID: 17105670
 52. Ates LS. New insights into the mycobacterial PE and PPE proteins provide a framework for future research. Mol Microbiol. 2020; 113(1):4–21. <https://doi.org/10.1111/mmi.14409> PMID: 31661176
 53. Korotkova N, Freire D, Phan TH, Ummels R, Creekmore CC, Evans TJ, et al. Structure of the Mycobacterium tuberculosis type VII secretion system chaperone EspG5 in complex with PE25–PPE41 dimer. Mol Microbiol. 2014; 94(2):367–82. <https://doi.org/10.1111/mmi.12770> PMID: 25155747
 54. Siegrist MS, Unnikrishnan M, McConnell MJ, Borowsky M, Cheng TY, Siddiqi N, et al. Mycobacterial Esx-3 is required for mycobactin-mediated iron acquisition. Proc Natl Acad Sci USA. 2009 Nov 3; 106(44):18792–7. <https://doi.org/10.1073/pnas.0900589106> PMID: 19846780
 55. Mitra A, Ko YH, Cingolani G, Niederweis M. Heme and hemoglobin utilization by Mycobacterium tuberculosis. Nat Commun. 2019 Sep 18; 10(1):4260. <https://doi.org/10.1038/s41467-019-12109-5> PMID: 31534126
 56. Ramakrishnan P, Aagesen AM, McKinney JD, Tischler AD. Mycobacterium tuberculosis resists stress by regulating PE19 expression. Infect Immun. 2016 Feb 24; 84(3):735–46.
 57. Qian J, Chen R, Wang H, Zhang X. Role of the PE/PPE Family in Host–Pathogen Interactions and Prospects for Anti-Tuberculosis Vaccine and Diagnostic Tool Design. Front Cell Infect Microbiol. 2020;10:10.3389/fcimb.2020.594288.
 58. Sassetti CM, Rubin EJ. Genetic requirements for mycobacterial survival during infection. Proc Natl Acad Sci USA. 2003 Oct 28; 100(22):12989–94. <https://doi.org/10.1073/pnas.2134250100> PMID: 14569030
 59. Jiang Y, Wei J, Liu H, Li G, Guo Q, Qiu Y, et al. Polymorphisms in the PE35 and PPE68 antigens in Mycobacterium tuberculosis strains may affect strain virulence and reflect ongoing immune evasion. Mol Med Rep. 2016 Jan 1; 13(1):947–54. <https://doi.org/10.3892/mmr.2015.4589> PMID: 26648016
 60. Ates LS, Dippenaar A, Ummels R, Piersma SR, van der Woude AD, van der Kuyj K, et al. Mutations in ppe38 block PE_PGRS secretion and increase virulence of Mycobacterium tuberculosis. Nat Microbiol. 2018 Feb; 3(2):181–8. <https://doi.org/10.1038/s41564-017-0090-6> PMID: 29335553
 61. Shah S, Cannon JR, Fenselau C, Briken V. A duplicated ESAT-6 region of ESX-5 Is Involved in protein export and virulence of mycobacteria. Infect Immun. 2015 Nov; 83(11):4349–61. <https://doi.org/10.1128/IAI.00827-15> PMID: 26303392

62. Saini NK, Baena A, Ng TW, Venkataswamy MM, Kennedy SC, Kunnath-Velayudhan S, et al. Suppression of autophagy and antigen presentation by *Mycobacterium tuberculosis* PE_PGRS47. *Nat Microbiol*. 2016 Aug 15; 1(9):1–12. <https://doi.org/10.1038/nmicrobiol.2016.133> PMID: 27562263
63. Wang Q, Boshoff HIM, Harrison JR, Ray PC, Green SR, Wyatt PG, et al. PE/PPE proteins mediate nutrient transport across the outer membrane of *Mycobacterium tuberculosis*. *Science*. 2020 Mar 6; 367(6482):1147–51. <https://doi.org/10.1126/science.aav5912> PMID: 32139546
64. Singh VK, Srivastava M, Dasgupta A, Singh MP, Srivastava R, Srivastava BS. Increased virulence of *Mycobacterium tuberculosis* H37Rv overexpressing LipY in a murine model. *Tuberculosis*. 2014 May 1; 94(3):252–61. <https://doi.org/10.1016/j.tube.2014.02.001> PMID: 24631199
65. McEvoy CRE, Warren RM, van Helden PD, Gey van Pittius NC. Multiple, independent, identical IS6110 insertions in *Mycobacterium tuberculosis* PPE genes. *Tuberculosis*. 2009 Nov 1; 89(6):439–42. <https://doi.org/10.1016/j.tube.2009.08.001> PMID: 19734099
66. Namouchi A, Karboul A, Fabre M, Gutierrez MC, Mardassi H. Evolution of smooth tubercle bacilli PE and PE_PGRS genes: Evidence for a prominent role of recombination and imprint of positive selection. *PLoS One*. 2013 May 21; 8(5):e64718. <https://doi.org/10.1371/journal.pone.0064718> PMID: 23705005
67. Bunduc CM, Ding Y, Kuijl C, Marlovits TC, Bitter W, Houben ENG. Reconstitution of a minimal ESX-5 type VII secretion system suggests a role for PPE proteins in the outer membrane transport of proteins. *mSphere*. 2023 Sep 25; 8(5):e00402–23. <https://doi.org/10.1128/msphere.00402-23> PMID: 37747201
68. Batt SM, Minnikin DE, Besra GS. The thick waxy coat of mycobacteria, a protective layer against antibiotics and the host's immune system. *Biochem J*. 2020 May 29; 477(10):1983–2006. <https://doi.org/10.1042/BCJ20200194> PMID: 32470138
69. Kwan DH, Sun Y, Schulz F, Hong H, Popovic B, Sim-Stark JC, et al. Prediction and manipulation of the stereochemistry of enoylreduction in modular polyketide synthases. *Chem Biol*. 2008 Nov 24; 15(11):1231–40. <https://doi.org/10.1016/j.chembiol.2008.09.012> PMID: 19022183
70. Daffe M, McNeil M, Brennan PJ. Novel type-specific lipooligosaccharides from *Mycobacterium tuberculosis*. *Biochemistry*. 1991 Jan 15; 30(2):378–88. <https://doi.org/10.1021/bi00216a011> PMID: 1899023
71. Belardinelli JM, Larrouy-Maumus G, Jones V, Carvalho LPS de, McNeil MR, Jackson M. Biosynthesis and translocation of unsulfated acyltrehaloses in *Mycobacterium tuberculosis*. *J Biol Chem*. 2014 Oct 3; 289(40):27952–65. <https://doi.org/10.1074/jbc.M114.581199> PMID: 25124040
72. Kalscheuer R, Koliwer-Brandl H. Genetics of mycobacterial trehalose metabolism. *Microbiol Spectr*. 2014;2(3):10.1128/microbiolspec.mgm2-0002–2013. <https://doi.org/10.1128/microbiolspec.MGM2-0002-2013> PMID: 26103976
73. Chopra T, Banerjee S, Gupta S, Yadav G, Anand S, Surolia A, et al. Novel intermolecular iterative mechanism for biosynthesis of mycoketide catalyzed by a bimodular polyketide synthase. *PLoS Biol*. 2008 Jul 8; 6(7):e163. <https://doi.org/10.1371/journal.pbio.0060163> PMID: 18613748
74. Angala SK, Belardinelli JM, Huc-Claustre E, Wheat WH, Jackson M. The cell envelope glycoconjugates of *Mycobacterium tuberculosis*. *Crit Rev Biochem Mol Biol*. 2014; 49(5):361–99. <https://doi.org/10.3109/10409238.2014.925420> PMID: 24915502
75. Quadri LEN. Biosynthesis of mycobacterial lipids by polyketide synthases and beyond. *Crit Rev Biochem Mol Biol*. 2014; 49(3):179–211. <https://doi.org/10.3109/10409238.2014.896859> PMID: 24625105
76. Ren H, Dover LG, Islam ST, Alexander DC, Chen JM, Besra GS, et al. Identification of the lipooligosaccharide biosynthetic gene cluster from *Mycobacterium marinum*. *Mol Microbiol*. 2007; 63(5):1345–59. <https://doi.org/10.1111/j.1365-2958.2007.05603.x> PMID: 17302813
77. Rombouts Y, Alibaud L, Carrère-Kremer S, Maes E, Tokarski C, Ellass E, et al. Fatty Acyl Chains of *Mycobacterium marinum* Lipooligosaccharides STRUCTURE, LOCALIZATION AND ACYLATION BY PapA4 (MMAR_2343) PROTEIN. *J Biol Chem*. 2011 Sep 23; 286(38):33678–88. <https://doi.org/10.1074/jbc.M111.273920> PMID: 21803773
78. Etienne G, Malaga W, Laval F, Lemassu A, Guilhot C, Daffé M. Identification of the Polyketide Synthase Involved in the Biosynthesis of the Surface-Exposed Lipooligosaccharides in *Mycobacteria*. *J Bact*. 2009 Apr 15; 191(8):2613–21. <https://doi.org/10.1128/JB.01235-08> PMID: 19181796
79. Ramakrishnan L, Tran HT, Federspiel NA, Falkow S. A crtB homolog essential for photochromogenicity in *Mycobacterium marinum*: isolation, characterization, and gene disruption via homologous recombination. *J Bact*. 1997 Sep 1; 179(18):5862–8. <https://doi.org/10.1128/jb.179.18.5862-5868.1997> PMID: 9294446
80. Thawornwiriyun P, Tanasupawat S, Dechsakulwatana C, Techkarnjanaruk S, Suntornsuk W. Identification of newly zeaxanthin-producing bacteria isolated from sponges in the Gulf of Thailand and

- their zeaxanthin production. *Appl Biochem Biotechnol*. 2012 Aug; 167(8):2357–68. <https://doi.org/10.1007/s12010-012-9760-2> PMID: 22715027
81. Maoka T. Carotenoids in marine animals. *Mar Drugs*. 2011 Feb 22; 9(2):278–93. <https://doi.org/10.3390/md9020278> PMID: 21566799
 82. Wilkie MEM, McShane H. TB vaccine development: where are we and why is it so difficult? *Thorax*. 2015 Mar 1; 70(3):299–301. <https://doi.org/10.1136/thoraxjnl-2014-205202> PMID: 25432943
 83. Hsu T, Hingley-Wilson SM, Chen B, Chen M, Dai AZ, Morin PM, et al. The primary mechanism of attenuation of bacillus Calmette–Guérin is a loss of secreted lytic function required for invasion of lung interstitial tissue. *Proc Natl Acad Sci USA*. 2003 Oct 14; 100(21):12420–5.
 84. Pym AS, Brodin P, Brosch R, Huerre M, Cole ST. Loss of RD1 contributed to the attenuation of the live tuberculosis vaccines *Mycobacterium bovis* BCG and *Mycobacterium microti*. *Mol Microbiol*. 2002; 46(3):709–17. <https://doi.org/10.1046/j.1365-2958.2002.03237.x> PMID: 12410828
 85. Pym AS, Brodin P, Majlessi L, Brosch R, Demangel C, Williams A, et al. Recombinant BCG exporting ESAT-6 confers enhanced protection against tuberculosis. *Nat Med*. 2003 May; 9(5):533–9. <https://doi.org/10.1038/nm859> PMID: 12692540
 86. Gröschel MI, Sayes F, Shin SJ, Frigui W, Pawlik A, Orgeur M, et al. Recombinant BCG Expressing ESX-1 of *Mycobacterium marinum* Combines Low Virulence with Cytosolic Immune Signaling and Improved TB Protection. *Cell Rep*. 2017 Mar 14; 18(11):2752–65. <https://doi.org/10.1016/j.celrep.2017.02.057> PMID: 28297677
 87. Muruganandah V, Sathkumara HD, Pai S, Rush CM, Brosch R, Waardenberg AJ, et al. A systematic approach to simultaneously evaluate safety, immunogenicity, and efficacy of novel tuberculosis vaccination strategies. *Sci Adv*. 2020 Mar 4; 6(10):eaaz1767. <https://doi.org/10.1126/sciadv.aaz1767> PMID: 32181361
 88. Kouprina N, Noskov VN, Larionov V. Selective isolation of large segments from individual microbial genomes and environmental DNA samples using transformation-associated recombination cloning in yeast. *Nat Protoc*. 2020 Mar; 15(3):734–49. <https://doi.org/10.1038/s41596-019-0280-1> PMID: 32005981
 89. Kim BJ, Kim BR, Kook YH, Kim BJ. A temperature sensitive *Mycobacterium paragordoniae* induces enhanced protective immune responses against mycobacterial infections in the mouse model. *Sci Rep*. 2017 Nov 9; 7(1):15230. <https://doi.org/10.1038/s41598-017-15458-7> PMID: 29123166
 90. Sayes F, Blanc C, Ates LS, Deboosere N, Orgeur M, Chevalier FL, et al. Multiplexed quantitation of intraphagocyte *Mycobacterium tuberculosis* secreted protein effectors. *Cell Rep*. 2018 Apr 24; 23(4):1072–84. <https://doi.org/10.1016/j.celrep.2018.03.125> PMID: 29694886
 91. Brown-Elliott BA, Simmer PJ, Trovato A, Hyle EP, Droz S, Buckwalter SP, et al. *Mycobacterium decipiens* sp. nov., a new species closely related to the *Mycobacterium tuberculosis* complex. *Int J Syst Evol Microbiol*. 2018; 68(11):3557–62.
 92. Turenne C, Chedore P, Wolfe J, Jamieson F, Broukhanski G, May K, et al. *Mycobacterium lacus* sp. nov., a novel slowly growing, non-chromogenic clinical isolate. *Int J Syst Evol Microbiol*. 2002; 52(6):2135–40.
 93. van Ingen J, Al-Hajj SAM, Boeree M, Al-Rabiah F, Enaimi M, de Zwaan R, et al. *Mycobacterium riyadhense* sp. nov., a non-tuberculous species identified as *Mycobacterium tuberculosis* complex by a commercial line-probe assay. *Int J Syst Evol Microbiol*. 2009; 59(5):1049–53.
 94. Saito H, Iwamoto T, Ohkusu K, Otsuka Y, Akiyama Y, Sato S, et al. *Mycobacterium shinjukuense* sp. nov., a slowly growing, non-chromogenic species isolated from human clinical specimens. *Int J Syst Evol Microbiol*. 2011; 61(8):1927–32.
 95. Pozzolini M, Scarfi S, Gallus L, Ferrando S, Cerrano C, Giovine M. Silica-induced fibrosis: an ancient response from the early metazoans. *J Exp Biol*. 2017 Nov 1; 220(21):4007–15. <https://doi.org/10.1242/jeb.166405> PMID: 29093191
 96. Brodin P, Majlessi L, Marsollier L, de Jonge MI, Bottai D, Demangel C, et al. Dissection of ESAT-6 system 1 of *Mycobacterium tuberculosis* and impact on immunogenicity and virulence. *Infect Immun*. 2006 Jan; 74(1):88–98.
 97. Chen JM, Zhang M, Rybniker J, Boy-Röttger S, Dhar N, Pojer F, et al. *Mycobacterium tuberculosis* EspB binds phospholipids and mediates EsxA-independent virulence. *Mol Microbiol*. 2013; 89(6):1154–66. <https://doi.org/10.1111/mmi.12336> PMID: 23869560
 98. Jain C, Rodriguez-R LM, Phillippy AM, Konstantinidis KT, Aluru S. High throughput ANI analysis of 90K prokaryotic genomes reveals clear species boundaries. *Nat Commun*. 2018 Nov 30; 9(1):5114. <https://doi.org/10.1038/s41467-018-07641-9> PMID: 30504855
 99. Page AJ, Cummins CA, Hunt M, Wong VK, Reuter S, Holden MTG, et al. Roary: rapid large-scale prokaryote pan genome analysis. *Bioinformatics*. 2015 Nov 15; 31(22):3691–3. <https://doi.org/10.1093/bioinformatics/btv421> PMID: 26198102

100. Minh BQ, Schmidt HA, Chernomor O, Schrempf D, Woodhams MD, von Haeseler A, et al. IQ-TREE 2: New models and efficient methods for phylogenetic inference in the genomic era. *Mol Biol Evol.* 2020 May 1; 37(5):1530–4. <https://doi.org/10.1093/molbev/msaa015> PMID: 32011700
101. Larkin MA, Blackshields G, Brown NP, Chenna R, McGettigan PA, McWilliam H, et al. Clustal W and Clustal X version 2.0. *Bioinformatics.* 2007 Nov 1; 23(21):2947–8. <https://doi.org/10.1093/bioinformatics/btm404> PMID: 17846036
102. Gilchrist CLM, Booth TJ, van Wersch B, van Grieken L, Medema MH, Chooi YH. cblaster: a remote search tool for rapid identification and visualization of homologous gene clusters. *Bioinfo Adv.* 2021 Jan 1;1(1):vbab016. <https://doi.org/10.1093/bioadv/vbab016> PMID: 36700093
103. Gilchrist CLM, Chooi YH. clinker & clustermap.js: automatic generation of gene cluster comparison figures. *Bioinformatics.* 2021 Aug 15; 37(16):2473–5.
104. Klatt S, Brammananth R, O'Callaghan S, Kouremenos KA, Tull D, Crellin PK, et al. Identification of novel lipid modifications and intermembrane dynamics in *Corynebacterium glutamicum* using high-resolution mass spectrometry [S]. *J Lipid Res.* 2018 Jan 1; 59(7):1190–204.
105. Hughes CS, Moggridge S, Müller T, Sorensen PH, Morin GB, Krijgsveld J. Single-pot, solid-phase-enhanced sample preparation for proteomics experiments. *Nat Protoc.* 2019 Jan; 14(1):68–85. <https://doi.org/10.1038/s41596-018-0082-x> PMID: 30464214
106. Ates LS, Sayes F, Frigui W, Ummels R, Damen MPM, Bottai D, et al. RD5-mediated lack of PE_PGRS and PPE-MPTR export in BCG vaccine strains results in strong reduction of antigenic repertoire but little impact on protection. *PLoS Pathog.* 2018 Jun 18; 14(6):e1007139. <https://doi.org/10.1371/journal.ppat.1007139> PMID: 29912964
107. Abdallah AM, Verboom T, Weerdenburg EM, Gey van Pittius NC, Mahasha PW, Jiménez C, et al. PPE and PE_PGRS proteins of *Mycobacterium marinum* are transported via the type VII secretion system ESX-5. *Mol Microbiol.* 2009; 73(3):329–40. <https://doi.org/10.1111/j.1365-2958.2009.06783.x> PMID: 19602152
108. Harboe M, Malin AS, Dockrell HS, Gotten Wiker H, Ulvund G, Holm A, et al. B-Cell Epitopes and Quantification of the ESAT-6 Protein of *Mycobacterium tuberculosis*. *Infect Immun.* 1998 Feb; 66(2):717–23. <https://doi.org/10.1128/IAI.66.2.717-723.1998> PMID: 9453632
109. Alderson MR, Bement T, Day CH, Zhu L, Molesh D, Skeiky YAW, et al. Expression cloning of an immunodominant family of mycobacterium tuberculosis antigens using human cd4+ t cells. *J Exp Med.* 2000 Feb 7; 191(3):551–60. <https://doi.org/10.1084/jem.191.3.551> PMID: 10662800
110. Parish T. Electroporation of Mycobacteria. In: Parish T, Kumar A, editors. *Mycobacteria Protocols* [Internet]. New York, NY: Springer US; 2021 [cited 2023 Sep 5]. p. 273–84. (Methods in Molecular Biology). Available from: 3
111. Wallace JR, Mangas KM, Porter JL, Marcsisin R, Pidot SJ, Howden B, et al. *Mycobacterium ulcerans* low infectious dose and mechanical transmission support insect bites and puncturing injuries in the spread of Buruli ulcer. *PLoS Negl Trop Dis.* 2017 Apr 14; 11(4):e0005553. <https://doi.org/10.1371/journal.pntd.0005553> PMID: 28410412
112. Stutz MD, Allison CC, Ojaimi S, Preston SP, Doerflinger M, Arandjelovic P, et al. Macrophage and neutrophil death programs differentially confer resistance to tuberculosis. *Immunity.* 2021 Aug 10; 54(8):1758–1771.e7. <https://doi.org/10.1016/j.immuni.2021.06.009> PMID: 34256013